# Constrained generalized predictive control of battery charging process based on a coupled thermoelectric model

Kailong Liu[a], Kang Li[a], Cheng Zhang[a]

[a] *School of Electronics, Electrical Engineering and Computer Science, Queen's University Belfast, Belfast, BT9 5AH, United Kingdom (Email:{kliu02,k.li,czhang07}@qub.ac.uk).*

**Abstract:** Battery temperature is a primary factor affecting the battery performance. Suitable battery temperature control, in particular internal temperature control can not only guarantee the battery operation safety but also improve its efficiency. This is however challenging as existing controller designs for battery charging rarely have a mechanism to incorporate such information. This paper proposes a novel battery charging control strategy which applies the constrained generalized predictive control (GPC) to charge a $LiFePO_4$ battery based on a newly developed coupled thermoelectric model. The control target primarily aims to maintain the battery internal temperature within a desirable range while delivering fast charging. To achieve this, the coupled thermoelectric model is firstly introduced to capture the battery behaviours in particular SOC and internal temperature which are not directly measurable. Then a controlled auto-regressive integrated moving average (CARIMA) model, whose structure is optimized by a fast recursive algorithm and the parameters are identified by the recursive least squares algorithm, is developed as an online self-tuning predictive model for a GPC controller. Then the constrained generalized predictive controller is developed to manipulate the charging current. Experiment results confirm the effectiveness of the proposed control strategy. Further, the best region of the heat dissipation rate and proper internal temperature set-points are investigated and analysed.

**Keywords:** $LiFePO_4$ battery; Constrained generalized predictive control; Coupled thermoelectric model; Battery internal temperature; Battery charging process

## 1. Introduction

To tackle the air pollutions and green-house gas emissions due to extensive consumption of fossil fuels from different sectors including the transportation, pure battery electric vehicles (EVs) and hybrid electric vehicles (HEVs) have attracted substantial interests in recent years to replace conventional internal combustion engine (ICE) based vehicles [1]. In this fast-growing area, high energy density and high specific power batteries are the focus in order to meet the operational requirements for electric vehicles. Among various types of batteries (e.g. lead-acid, nickel metal/Ni-MH and metal/air), lithium-ion (Li-ion) battery is widely used as power supplies in electric vehicles due to its excellent performance in terms of power densities, longevity and environmental

characteristics. Operation safety of Li-ion batteries is a key issue for electric vehicles, and a high performance battery management system (BMS) which consists of distributed sensors and control units is essential in protecting batteries from damages due to detrimental operation conditions, ensuring batteries operate within safe environment and prolonging their service life [2].

Battery thermal management is a kernel part of the BMS. Temperature affects battery performance in many ways such as round trip efficiency, energy and power capability, cycle life, reliability and charge acceptance [3]. Both the surface temperature and internal temperature may exceed permissible levels when batteries charge or discharge at prevailing conditions or at high ambient temperature, which is detrimental for battery operation safety and will dramatically decrease the battery performance. On the other hand, if the battery temperature exceeds a certain minimum threshold, it starts to generate heat uncontrollably while in operation [4]. The battery capacity will be lost irreversibly if charging battery at low temperature due to poor charge transfer at the electrode/electrolyte interface [5]. Therefore, suitable battery thermal management which monitors and controls the battery temperature is indispensable in EV applications [6].

To date, the reasonable working temperature suitable for most current Li-ion batteries is to charge between 0-45ºC and discharge between -20-60 ºC based on the instruction manuals from most battery manufacturers. A number of effective approaches have been proposed to estimate, monitor and control the temperature and to guarantee Li-ion battery operation safety [3]. In terms of battery materials, novel electrolytes materials, and anode and cathode materials which can improve operation safety for Li-ion batteries under high temperature circumstance have been researched. Maleki et al. [7] researched high thermal Li-ion conductivity cells based on negative electrode material with high thermal conductive property. Kise et al. [8] presented a novel electrode which can improve safety for Li-ion batteries at high temperatures. For battery packages, researches are mainly focused on developing passive (i.e., using ambient environment) or active (i.e., an embedded source provides heating or cooling) systems to control the battery temperature under different situations. Based on the medium used, these systems can be further grouped as thermal management system using air [9], liquid [10], phase change materials [11], and combination of these mediums [12].

Furthermore, some researchers focus on the development of electronical circuits and a temperature management function is often embedded in the circuits. Park et al. [13] proposed a dynamic thermal model for the Li-ion battery system using the finite-volume approach. The thermal model is a two-state lumped model where the Joule heat is applied to calculate the heat generation. A battery cooling system with the cooling fan was then

developed under the battery charging and discharging processes. In [14], the relationship between the Li-ion BMS and charging strategies with temperature was analysed, and it has been shown that the battery temperature has a significant impact on the charging strategy design. A Li-ion battery protection approach was then proposed based on the existing integrated circuit (IC) conditions. Kim et al. in [15] analysed the effect of power requirements and temperature change on the electrical states of battery cells, and a battery thermal management architecture to heat/cool battery cells timely and selectively was proposed to improve the efficiency of the BMS.

To design effective control strategies for battery management has been another active research topic. Jiang et al. [16] proposed to adjust the charging current acceptance with different battery state of charge (SOC) stages using a constant-polarization-based fuzzy-control charging method to shorten the charging time. Liu et al. [17] presented an optimal five-step charging strategy for Li-ion batteries based on consecutive orthogonal arrays. Hu et al. [18] developed a dual-objective optimal charging strategy for lithium nickel-manganese-cobalt oxide (LiNMC) and lithium iron phosphate ($LiFePO_4$) batteries which optimally trades off the conflict between the energy loss and charging time.

It is clear that most control strategies adapt the charging current acceptance with battery SOC stages. However, little has been done so far to apply advanced control strategies that manipulate charging currents for battery thermal management. Klein et al. [19] used a nonlinear model predictive control (MPC) method to minimize a battery charging time based on the complex electrochemical model. Marcelo et al. [20] applied constrained MPC to generate battery CCCV charge current profile to charge a Li-ion battery cell as fast as possible. In these papers, MPC strategy has been successfully applied to BMS, but they mainly consider constraints on the charging current and voltage, as well as average shell temperature of battery, the temperatures especially the internal temperature of battery are not considered. This battery internal temperature control is however crucial in many prevailing battery application conditions. When batteries are charged with high current in order to reach the specified SOC as quickly as possible in high power applications, both the battery shell and internal temperature will increase noticeably. When the battery temperature exceeds the reliable operating range, battery performance will be severely damaged and even lead to battery failures and safety problems. Further, there exists large difference between the battery surface and internal temperature during charging process (e.g., sometimes greater than 10°C in high power applications [21]). The battery internal temperature usually increases to a critical temperature point earlier than the battery surface temperature. Therefore, the battery temperature especially the internal temperature has to be taken into account when batteries are charged with

high currents in high power applications. In other word, the battery internal temperature has to be controlled within certain range during the charging process.

One approach to achieve this is through the implementation of the generalized predictive control (GPC) assisted with a proper battery model which can not only reflect the battery electric behaviours but also the surface and internal temperature. GPC is a self-adapted control algorithm widely used in industrial applications [22]. According to 'look-ahead' strategy in GPC, the future outputs can be predicted at each sampling instant effectively. More importantly, GPC is able to calculate the suitable control increments with the constraints imposed on both the inputs and the outputs. This implies that hard constraints such as voltage, current and current increment limits which affect the battery performance can be incorporated into the battery thermal control strategy directly.

On the other hand, many researchers have focused on developing various battery thermal-electrical models. Lin et al. [23] proposed an one-dimensional thermal-electrochemical model to comprehensively investigate the effects of solid electrolyte interphase (SEI) growth on battery performance. Chao et al. [24] introduced a coupled mechanical-electrical-thermal model for battery simulation to better understand the behaviour of Li-ion batteries under mechanical abuse. Marie-Therese et al. [25] proposed a phenomenological equivalent circuit model for a Li-ion battery to account for the local electrochemical and thermal behaviour, variable double layer capacitance and degradation. These developed models have significantly improved the understanding of the battery charging and discharging processes, though most of them are generally too complex to be used in real-time control. In this paper, we aim to develop advanced control method for battery charging, with particular consideration of the battery internal temperature for safety operation. Therefore, a proper and simplified battery thermoelectric model plays a vital role in designing a highly efficient control strategy and should be adopted. Our previous work [26] has shown a successful development of a coupled battery thermoelectric model. With some improvements of this thermoelectric model and the proposed constrained GPC strategy, the battery behaviours under a given internal temperature and SOC, which are often difficult to measure directly can now be estimated and controlled, and real world constraints on the battery operation can all be incorporated.

In summary, for the proposed strategy, the constrained GPC is first used to charge a battery from an initial SOC to a targeted state as quickly as possible, while keeping the battery internal temperature within an acceptable range during the charging process so as to enhance the battery safety and to avoid damages caused by overheating. Further, both battery electrical and thermal constraints including SOC, voltage, current and

temperature during operation are also incorporated into the control strategy. The main contributions of this work are summarized as follows: (1) The proposed fast charging control strategy considers the battery internal temperature which is important for safe operation and control of electric vehicles, particularly in some high power applications where the difference between surface temperature and internal temperature can be quite large. (2) The improved battery thermoelectric model in the charging control strategy can guarantee both charging efficiency and control of internal temperature rising to prolong battery service life. (3) The CARIMA model structure is optimized by a fast recursive algorithm (FRA). This brings extra benefits in that the model complexity is optimized so that the CARIMA model used in the GPC can be simplified with good performance and the computation time can be shortened in the implementation of the GPC controller. (4) The correlation between battery cooling cost and charging time during the charging process is analysed to identify the most appropriate region of heat dissipation rates. (5) The effect of internal temperature set-points on both charging time and energy loss is investigated to identify the proper internal temperature set-points.

The remainder of this paper is organized as follows. Section 2 first introduces relevant basics of Li-ion battery especially $LiFePO_4$ battery, in particular their temperature constraints, then the improved coupled thermoelectric model is presented. Section 3 develops the constrained GPC algorithm, especially the predictive model identification and constraints formulation. Details to formulate the battery charging control objectives, coupled thermoelectric model identification, and battery charging control strategy are presented in Section 4. Section 5 gives the experiment results to demonstrate the efficacy of the proposed approach. The most appropriate region of heat dissipation rates and battery internal temperature set-point are also investigated and analysed. Finally, section 6 concludes the paper.

## 2. Battery coupled thermoelectric model

In this section, the relevant basics of Li-ion battery especially $LiFePO_4$ battery, in particular their temperature constraints are presented firstly, followed by the illustration of the improved battery coupled thermoelectric model.

### 2.1 Basics of $LiFePO_4$ battery

$LiFePO_4$ battery uses nano-scale phosphate cathode materials to offer good electrochemical performance with low resistance. Particular characteristics of $LiFePO_4$ battery are shown in Table 1. $LiFePO_4$ is more tolerant to full charge condition and is less stressed than other Li-ion systems if being kept charging at high voltage.

[Table 1 about here.]

$LiFePO_4$ battery is now widely used in electric vehicles to replace the lead acid battery. Eq. (1)-(2) describe the chemical reactions occur during charging process. It should be noted that it is vital to control the $LiFePO_4$ battery charging process as it directly impacts the battery safety and performance.

$$LiFePO_4 \xrightarrow{Charge} yLi^+ + ye^- + Li_{1-y}FePo4 \quad \text{for positive electrode} \quad (1)$$

$$xLi^+ + xe^- + Li_{1-x}C_6 \xrightarrow{Charge} LiC_6 \quad \text{for negative electrode} \quad (2)$$

Conventional charging methods include current control, voltage control and Mas Law control [27]. Current control uses a small current to charge battery to avoid sharp increase in both battery temperature and voltage. However, this method is difficult to generate a suitable charging current rate for battery capacity balancing and to further ensure operation safety. For voltage control method, battery is charged at a constant voltage in order to avoid overvoltage problem which may occur at the end of charging process. The disadvantage of this method is that the current at the beginning of charging process may be too high, which can harm the battery life. The Mas Law method calculates the current to charge the battery by 'Mas Three Laws', but it is only designed for lead-acid batteries, not for Li-ion batteries.

The constant-current-constant-voltage (CCCV) method integrates current control and voltage control method to shorten charging time as well as to improve charging performance and safety [28]. In this method, battery is first charged at a constant current and the voltage increases due to the charge current. When the battery terminal voltage reaches the maximum safe value, the battery begins to be charged at a constant voltage until the battery capacity meets the goal requirement. Although CCCV is easy to apply, it is often designed using the voltage limits and thus may not take full advantage of the actual operating characteristics of batteries. Besides, both the shell and core temperature may exceed acceptable ranges when the battery is charged in high power applications without any other solutions. It is therefore vital to include the temperature information when battery is charged using CCCV method for some high power cases.

### 2.2 Battery temperature constraints

The reasonable ambient temperature limits for various batteries during charging or discharging process are shown in Table 2 [27]. Compared with Lead acid and NiMH/NiCd battery, Li-ion batteries have fairly desirable charging performance at cooler temperatures within the range of 0 to 45°C (41 to 113°F). During the charging process, the battery internal resistance will usually cause a slight temperature rise within the battery, and this

temperature rise will be more significant in cold environment due to the increase of the internal resistance. On the other hand, the battery internal resistance can be reduced by elevating the battery temperature, thus increase the Li-ion battery charging effectiveness slightly, but excessive high temperature will dramatically reduce the battery life. To achieve the best performance, Li-ion batteries are recommended to be charged within a narrower ambient temperature range of 10°C and 30°C (50°F and 86°F).

[Table 2 about here.]

Apart from the ambient temperature, the internal and surface temperatures of Li-ion batteries also impact the battery behaviour during the charging process. In our previous study [26], it is clearly shown that the battery internal and shell temperatures are distinctively different from ambient temperature during the fast charging process. The battery internal temperature is always higher and the difference between the internal and shell temperatures can be even more dramatical, which has revealed the importance to effectively control the battery internal temperature in order to prevent Li-ion battery from overheating during the charging process.

### 2.3 Battery coupled thermoelectric model

In the battery charging process, some battery internal states such as SOC and internal temperature are difficult to measure directly, yet they play vital roles for battery online status control and to ensure safe operation. In this paper, a newly developed thermoelectric model is used to capture both the battery thermal and electric behaviours, including voltage, surface temperature, and in particular SOC and internal temperature during battery charging. Then according to the comprehensive capture of the battery behaviours using this thermoelectric model, the constrained GPC strategy enables simultaneous and efficient control to guarantee both battery charging efficiency and internal temperature rising within reasonable ranges, further to prolong the battery service life.

#### 2.3.1 Battery electric circuit model

Different battery models including electrochemical models, equivalent electric circuit models, empirical models and reduced-order models have been proposed for different applications [29]. For $LiFePO_4$ battery cells, the first-order RC model [30], namely the Thevenin model, has been widely used in industrial applications due to its simple circuitry representation and easy to configure and identify the parameters compared to other mechanism models. In this paper, the Thevenin model, as shown in Fig. 1, is chosen as the battery electric model to describe the charging behaviour of Li-ion batteries.

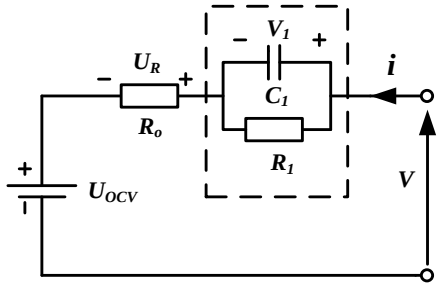


**Fig. 1.** Battery Thevenin model.

In the Thevenin model, $U_{OCV}$ is the battery open circuit voltage which is equivalent to electromotive force. The inherent conductivity is expressed by an ohmic resistance $R_o$, and a RC network is used to describe the battery polarization. The electrical potential balance is described by

$$V = V_1 + i * R_o + U_{OCV} \tag{3}$$

where $V$ is the battery terminal voltage and $i$ is the battery current. $V_1$ is the voltage of the RC network, which is also called the battery polarization voltage. $R_o$ represents battery internal resistance.

The battery SOC is calculated based on the battery nominal capacity shown as follows,

$$\mathrm{soc}(k) = \mathrm{soc}(k-1) - \frac{T_s}{C_n} * i(k-1) \tag{4}$$

where $C_n$ is the battery nominal capacity which unit is As (3600 As=1 Ah) and $T_s$ is the sampling time period which unit is second respectively.

Suppose the terminal load current keeps constant during the sampling period, then, following the dynamics of a RC network, the battery polarization voltage $V_1$ of RC network could be calculated as,

$$V_1(k) = \exp\left(-\frac{\Delta T}{R_1 C_1}\right) * V_1(k-1) - R_1\left(1 - \exp\left(-\frac{\Delta T}{R_1 C_1}\right)\right) * i(k-1)$$

$$= a_1 * V_1(k-1) - b_1 * i(k-1) \tag{5}$$

Combing equations (3)-(5), the battery Thevenin model can be expressed as follows:

$$\begin{cases} \mathrm{soc}(k) = \mathrm{sco}(k-1) - T_s/C_n * i(k-1) \\ V_1(k) = a_1 * V_1(k-1) - b_1 * i(k-1) \\ V(k) = V_1(k) + i(k) * R_o + U_{OCV} \end{cases} \tag{6}$$

where $R_o$ and $U_{OCV}$ are dependent on internal temperature and SOC respectively shown in Eq.(7)-(8). Both of them can be obtained from a look-up table based on linear interpolation algorithm.

$$R_o = f_R(T_{in}) \tag{7}$$

$$U_{OCV} = f_{ocv}(SOC) \tag{8}$$

#### 2.3.2 Battery lumped thermal model

Assuming the battery shell temperature and internal temperature are both uniform, and heat generation is uniformly distributed within the battery. Heat conduction is assumed to be the only heat transfer form between the battery core and shell, and also between the battery shell and the ambience, a two-stage approximation of the radially distributed thermal model for the battery cells can be defined as,

$$C_1 * \dot{T}_{in} = Q + \frac{(T_{sh} - T_{in})}{R_e}$$

$$= Q + k_1 * (T_{sh} - T_{in}) \tag{9}$$

$$C_2 * \dot{T}_{sh} = \frac{T_{in} - T_{sh}}{R_c} + \frac{(T_{amb} - T_{sh})}{R_u}$$

$$= k_1 * (T_{in} - T_{sh}) + k_2 * (T_{amb} - T_{sh}) \tag{10}$$

where the two states are the battery shell temperature $T_{sh}$ and the battery internal temperature $T_{in}$ respectively. $T_{amb}$ is the battery ambient temperature. $C_1$ is the heat capacity inside the cell and $C_2$ is the heat capacity of the battery casing. $Q$ stands for the generated heat within the battery during the charging/discharging process. $R_c$ is a lumped parameter gathering the conduction and contact thermal resistance across the compact materials. $R_u$ is a convection resistance to account for the convective heat transfer between the battery surface and the surrounding atmosphere. $k_1$ , $k_2$ both stand for the heat dissipation rate.

For the heat generation part $Q$, two typical ways [31,34] to calculate the heat generation are given below,

$$\begin{cases} Q_1 = i^2 * R_o \\ Q_2 = i * (v - U_{OCV}) + i * T_{in} * dU_{OCV}/dT_{in} \end{cases} \tag{11}$$

where $R_o$ is the battery internal resistance; $Q_1$ considers the heat generation is mainly dominated by the ohmic heat generated over internal resistance. $Q_2$ considers the heat generation caused by the over-potentials and entropy change within battery.

Assuming $\dot{T}(k+1) = \frac{z-1}{T_s} * T(k) = \frac{1}{T_s} * (T(k+1) - T(k))$, the two-stage thermal model for the battery cells can then be formulated as

$$\begin{cases} T_{in}(k+1) = \left(1 - T_s * \frac{k_1}{C_1}\right) * T_{in}(k) + T_s * \frac{k_1}{C_1} * T_{sh}(k) + \frac{T_s}{C_1} * Q \\ T_{sh}(k+1) = T_s * \frac{k_1}{C_2} * T_{in}(k) + \left(1 - T_s * \frac{k_1+k_2}{C_1}\right) * T_{sh}(k) + k_2 * T_{amb} * \frac{T_s}{C_2} \end{cases} \quad (12)$$

As the ambient temperature decreases or battery shell temperature rises, $k_2$ will increase accordingly and more heat be dissipated into the ambience [32], i.e. $k_2$ increases with the temperature gradient $T_{sh} - T_{amb}$. In order to take this effect into consideration and further improve the accuracy of the thermal model, two cases are considered and compared: 1) constant $k_2$; 2) time-varying $k_2$: $k_2 = k_{2,1} + k_{2,2} * (T_{sh} - T_{amb})$.

**Battery coupled thermoelectric model**

The battery Thevenin model and the two-stage thermal model are combined to produce the coupled thermoelectric model as follows,

$$\begin{cases} x(k+1) = A * x(k) + B(k) \\ V(k) = V_1(k) + f_R\left(T_{in}(k)\right) * i(k) + f_{ocv}(SOC(k)) \end{cases} \quad (13)$$

where

$$x(k) = [SOC(k), V_1(k), T_{in}(k), T_{sh}(k)]^T$$

$$\mathrm{A} = \begin{bmatrix} 1 & 0 & 0 & 0 \\ 0 & a_1 & 0 & 0 \\ 0 & 0 & 1 - T_s * k_1/C_1 & T_s * k_1/C_1 \\ 0 & 0 & T_s * k_1/C_2 & 1 - T_s * (k_1 + k_2)/C_2 \end{bmatrix}$$

$$B(k) = [-T_s/C_n * i(k), -b_1 * i(k), \quad Q * T_s/C_1, \quad k_2 * T_{amb} * T_s/C_2]^T$$

Compared with the battery electric sub-model or the thermal sub-model alone, the above thermoelectric model couples both the battery electric and thermal behaviours simultaneously. Given this advantage, this thermoelectric model is used to capture the battery behaviours, including voltage, surface temperature, and in particular SOC and internal temperature, which are not directly measurable in real-time applications. Given

these above, a constrained GPC strategy is then applied to charge a battery from an initial SOC to a targeted state, while to maintain the battery temperature within an acceptable range. Further, both battery electrical and thermal constraints are also considered in the controller design.

## 3. Constrained generalized predictive control

### 3.1 Fundamental principles

Generalized predictive control (GPC) belongs to a wide range of MPC algorithms. It formulates the optimization process of a suitable cost function concerning the future output errors and control actions. Compared with traditional control approach, GPC offers some advantages such as capability of stabilizing non-minimum phase and unstable open-loop processes, and handling unknown or variable dead-time and plants with unknown orders. Over the years, the GPC strategy has proven to be highly effective in many industrial applications where the performance and robustness are difficult to achieve with traditional designs. Besides, the hard constraints can be incorporated into the controller directly and solved by a quadratic optimization problem in GPC.

### 3.2 Predictive model identification

When applying the constrained GPC strategy for the battery charging process, the first task is to select a suitable predictive model to represent the controlled dynamic process. In order to improve the robustness of GPC controller, an online self-tuning predictive model is formulated using the controlled auto-regressive integrated moving average (CARIMA) model shown as follows,

$$A(z^{-1})y(k) = z^{-d}B(z^{-1})u(k) + \frac{1}{\Delta}C(z^{-1})\varepsilon(k) \tag{14}$$

where u$(k)$, y$(k)$ and $\varepsilon(k)$ are $m * 1$ input vector, $n * 1$ output vector and $n * 1$ noise vector at sampling time $k$ respectively. The noise in CARIMA model is supposed to be a zero mean white noise. $d$ is the delay factor and $\Delta = 1 - z^{-1}$ is a difference operator. $B(z^{-1})$ is a $n * m$ polynomial matrix, $A(z^{-1})$ and $C(z^{-1})$ are $n * n$ polynomial matrices defined respectively as follows.

$$\begin{cases} A(z^{-1}) = \mathrm{I}_{n\times n} + A_1 z^{-1} + A_2 z^{-2} + \cdots + A_{n_a} z^{-n_a} \\ B(z^{-1}) = B_0 + B_1 z^{-1} + B_2 z^{-2} + \cdots + B_{n_b} z^{-n_b} \\ C(z^{-1}) = \mathrm{I}_{n\times n} + C_1 z^{-1} + C_2 z^{-2} + \cdots + C_{n_c} z^{-n_c} \end{cases} \tag{15}$$

In our battery predictive model, the polynomial matrix $C(z^{-1})$ is set as an identity matrix $\mathrm{I}_{n\times n}$ for easy computation of each control increment. Multiplying $\Delta$ on each side of Eq. (15), the CARIMA model can be expressed as follows,

$$\Delta y(k) = \varphi^T(k)\theta + \varepsilon(k) \tag{16}$$

where $\Delta \mathrm{y}(k)$ is the vector of the current output increment obtained from the battery coupled thermoelectric model, $\varphi(k) = [-\Delta y(k-1), \dots, -\Delta y(k-n_a), \Delta u(k-1), \dots, \Delta u(k-n_b-1)]^T$ is a vector of past input and output increments and $\varepsilon(k)$ is the white noise. $\theta = [a_1, \dots, a_{n_a}, b_0, \dots, b_{n_b}]^T$ stands for the estimated parameter vectors. Both $\Delta y(k)$ and $\varphi(k)$ can be obtained in each sampling time, therefore to find the optimal $\theta$ in (16) becomes a typical least square (LS) problem in model identification if the cost function is defined as the sum of squared errors. In order to achieve online self-tuning, the parameters $\theta$ need to be identified using a recursive least squares (RLS) identification algorithm with forgetting factor $\lambda$ shown as follows,

$$\begin{cases} \hat{\theta}(k) = \hat{\theta}(k-1) + K(k)[\Delta y(k) - \varphi^T(k)\hat{\theta}(k-1)] \\ K(k) = P(k-1)\varphi(k)[\lambda + \varphi^T(k)P(k-1)\varphi(k)]^{-1} \\ P(k) = \lambda^{-1}\left[\mathrm{I} - K(k)\varphi^T(k)\right]P(k-1) \end{cases} \tag{17}$$

In each sampling time, the parameters $\theta$ can be updated by Eq. (17), so for a nonlinear system, the parameters $\theta$ in the predictive model can be updated in real time and it formulates a self-tuning process. The role of the forgetting factor $\lambda$ is to give the original and new data different weights, so the RLS algorithm can track the variation of the system behaviours quickly during the battery charging process.

### 3.3 *J*-step prediction outputs

Once the CARIMA model is obtained, the *j*-step prediction outputs need to be calculated in order to minimize the prediction error variance. The minimum j-step optimal prediction $y(k+j|k)$ can be derived from the difference equation as follows.

$$C(z^{-1})y(k+j|k) = G_j(z^{-1})y(k) + F_j(z^{-1})\Delta u(k+j-1) \tag{18}$$

where $G_j(z^{-1})$ and $F_j(z^{-1})$ are polynomial matrices which need to satisfy following Diophantine equation

$$\begin{cases} C(z^{-1}) = A(z^{-1})\Delta E_j(z^{-1}) + z^{-j}G_j(z^{-1}) \\ F_j(z^{-1}) = B(z^{-1})E_j(z^{-1}) \end{cases} \tag{19}$$

After the corresponding polynomial matrices in Eq. (19) are obtained, the *j*-step prediction can thus be derived as follows:

$$\mathbf{Y} = \mathbf{G}\Delta\boldsymbol{U} + \mathbf{F} \tag{20}$$

where $\mathbf{Y} = [\hat{y}(k+j|t) \ \ldots \ \hat{y}(k+N_P|t)]^{\boldsymbol{T}}$, $\Delta\boldsymbol{U} = [\Delta u(k) \ \ldots \ \Delta u(k+N_C-1)]^{\boldsymbol{T}}$, $\mathbf{F} = [f_{\mathbf{1}} \ldots f_{\boldsymbol{N_P}}]^{\boldsymbol{T}}$

$$\mathbf{G} = \begin{bmatrix} G_0 & 0 & \cdots & 0 & \cdots & 0 \\ G_1 & G_0 & \cdots & 0 & \cdots & 0 \\ \vdots & \vdots & \ddots & \vdots & \vdots & \vdots \\ G_{j-1} & G_{j-2} & \cdots & G_0 & \vdots & 0 \\ \vdots & \vdots & \vdots & \vdots & \ddots & \vdots \\ G_{N_y-1} & G_{N_y-2} & \cdots & \cdots & \cdots & G_0 \end{bmatrix}$$

### 3.4 Constrained formulation

The predictive control sequence can be obtained by minimizing a multistage cost function of the following form:

$$\begin{aligned} J = &\textstyle\sum_{j=1}^{N_P}[\hat{y}(k+j|k) - y_r(k+j)]^T\, Q\,[\hat{y}(k+j|k) - y_r(k+j)] \\ &+ \textstyle\sum_{j=1}^{N_C} \Delta u(k+j-1)^T R \Delta u(k+j-1) \end{aligned} \tag{21}$$

where $N_P$ is the prediction horizon and $N_C$ is the control horizon respectively. $Q$ and $R$ stand for weights on the error vector and control vector respectively in order to constrain the future tracking errors and control efforts along the horizons. $y_r(k+j)$ is the set-point sequence for the reference system output vector. $\hat{y}(k+j|k)$ is the optimal j-step prediction for the model output up to time $k$. $\Delta u(k+\mathrm{j}-1) = u(k+\mathrm{j}-1) - u(k+\mathrm{j}-2)$ is the future control increment sequence. Tuning parameters for the horizons and weights are the key in designing the controller.

When the input and output constraints are incorporated into the control formulation, then the optimal solution of cost function Eq. (21) have to fall within the feasible region defined by the constraints. Inequalities Eq. (22) and Eq. (23) stipulate the input constraints. Besides, the output constraints which are formulated by inequality Eq. (24) need to be used to confine the control actions within the reliable operating region.

$$u_{min} \le u(k) \le u_{max} \tag{22}$$

$$-\Delta u_{max} \le \Delta u(k) \le \Delta u_{max} \tag{23}$$

where $u_{min}$ and $u_{max}$ are the minimum and maximum input values respectively and $\Delta u_{max}$ stands for the maximum rate of control input.

$$y_{min} \le y(k) \le y_{max} \tag{24}$$

where $y_{min}$ and $y_{max}$ are the minimum and maximum output values respectively.

Substituting the prediction equation Eq. (20) into the cost function Eq. (21), the objective function can be reformulated as:

$$\begin{aligned} J &= \frac{1}{2}\Delta \boldsymbol{U}^T(k)\cdot \boldsymbol{2}\cdot[\boldsymbol{G}^T Q\boldsymbol{G}+R]\Delta \boldsymbol{U}(k)+\left[2\boldsymbol{G}^T Q\left(\boldsymbol{F}-y_r(k+1)\right)\right]^T\Delta \boldsymbol{U}(k)+C \\ &= \frac{1}{2}\Delta \boldsymbol{U}^T(k)\boldsymbol{H}\Delta \boldsymbol{U}(k)+g^T\Delta \boldsymbol{U}(k)+C \end{aligned} \tag{25}$$

where $C=[\boldsymbol{F}-y_r(k+1)]^T Q[\boldsymbol{F}-y_r(k+1)]$ is a constant term.

In order to formulate a quadratic objective function and employ popular solvers for quadratic programming to solve the constrained control problem, the inequalities (22), (23) and (24) should be reformulated as

$$L\Delta \boldsymbol{U}\le D \tag{26}$$

where $=\begin{bmatrix} \mathrm{I}_1 \\ -C_1 \\ C_1 \\ -G \\ G \end{bmatrix}$, $D=\begin{bmatrix} B\Delta u_{max} \\ -Bu_{min}+Bu(k-1) \\ Bu_{max}-Bu(k-1) \\ -B_n y_{min}+F \\ B_n y_{max}-F \end{bmatrix}$, $C_1=\begin{bmatrix} \mathrm{I}_2 & 0 & 0 & 0 \\ \mathrm{I}_2 & \mathrm{I}_2 & 0 & 0 \\ \vdots & \vdots & \ddots & 0 \\ \mathrm{I}_2 & \mathrm{I}_2 & \cdots & \mathrm{I}_2 \end{bmatrix}_{N_C\times N_C}$

$\mathrm{I}_1=\mathrm{I}_{(m\times N_C)\times(m\times N_C)}$, $\mathrm{I}_2=\mathrm{I}_{(m\times m)}$, $\mathrm{I}_3=\mathrm{I}_{(n\times n)}$, $B=\underbrace{[\mathrm{I}_2 \quad \mathrm{I}_2 \quad \cdots \quad \mathrm{I}_2]^T}_{N_C}$ and $B_n=\underbrace{[\mathrm{I}_3 \quad \mathrm{I}_3 \quad \cdots \quad \mathrm{I}_3]^T}_{N_P}$. $m$, $n$ are the number of inputs and outputs respectively. $N_P$, $N_C$ are the prediction horizon and control horizon respectively.

## 4. Constrained GPC for battery temperature control

### 4.1 Control objectives for battery charging process

Constrained GPC will be first used in battery charging with the target to keep the battery temperature especially for the internal temperature within acceptable ranges while fast charging the battery. Hard constraints should be also considered during the charging process. The constrained GPC strategy for battery charging process is shown in Fig. 2. The main control objective is to keep each measured process output $T_{in}(k)$ as close as possible to its set-points $T_{in}\_r(k)$. Besides, the hard constraints for terminal voltage $V$, battery shell temperature $T_{sh}$, battery SOC, and battery charging input current $i$ are also considered.

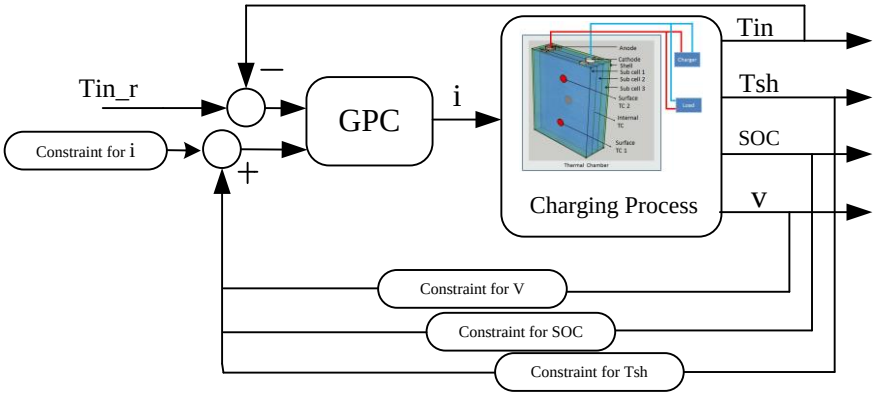


**Fig. 2.** Constrained GPC for battery charging

To ensure that the battery charging is operated efficiently within the safety region, the current controller for the battery needs to meet the following requirements:

(1). The battery SOC must meet the EV application demand.

(2). The terminal voltage must be operated within reliable and safe operating range to avoid high voltage situation which will accelerate the capacity loss, resulting in internal short circuits as well as decomposition of the electrolyte.

(3). Both the temperatures of battery shell and core must be maintained within a desired level to ensure proper and safe charging, avoiding battery service life being shortened or terminated and battery thermal runaway caused by over-temperature.

(4). The battery SOC should be charged from initial SOC state to a specified state as fast as possible under the above mentioned constraints.

### 4.2 Thermoelectric model identification

To apply constrained GPC strategy for the battery thermal management, it is necessary to identify its thermoelectric model based on test and measurement data. Under laboratory test conditions, a Li-ion battery cell which has a nominal capacity of 10Ah and a nominal operation voltage of 3.2V was used in this study. The electric model parameters were identified through the least square method based on measured battery terminal current, voltage and the thermal model parameters were also acquitted through the least square method based on battery self-heating test data respectively. The detailed identification process could be referred to our previous work [26] and will be not repeated in this paper due to page limit.

The battery OCV with SOC is shown in Table 3, and their relation $U_{OCV} = f_{ocv}(SOC)$ is calculated by the linear interpolation method. The battery internal resistance $R_o$ is calculated under different internal temperature $T_{in}$, and the relationship for $R_o = f_R(T_{in})$ at different internal temperature is shown in Table 4.

[Table 3 about here.]

[Table 4 about here.]

The identified parameters of the improved thermoelectric model are listed in Table 5. The identified model was further validated, and for the electric part, the maximum validation voltage error is less than 50mV (2.1% of battery nominal voltage), and the root mean square error (RMSE) is about 3.4mV, the detailed validation results can be found in [26]. For the improved thermal part, the validation results are presented in Section 5 in detail. These modelling errors are acceptable for the design of a suitable battery charging control strategy in this study.

[Table 5 about here.]

#### 4.3 Battery charging controller design

Following the introductions of section 2.3 and section 4.2, we first produce the constraints for battery charging process based on the identified thermoelectric model. The applied current is limited for 3C rates based on the battery properties. The hard constraints of both the terminal voltage and current are given as follows,

$$-30\ \text{A} \le i(k) \le 0\ \text{A} \qquad \text{for 3C ;} \tag{27}$$

$$2.6\ \text{V} \le \text{V}(k) \le 3.65\ \text{V} \tag{28}$$

Suppose the charging process starts from initial SOC of 0.1, and the targeted state is 0.9, that is

$$0.1 \le \text{SOC}(k) \le 0.9 \tag{29}$$

The main control target is to find a suitable charging current profile $i(k)$ that could maintain the battery temperature within a desired level while driving the SOC from initial state 0.1 to final state 0.9 simultaneously. The hard constraints for voltage and current should be also considered during the charging process. According to the constrained GPC strategy, the optimal increment sequence $\Delta i(k)$ of control inputs (charging current) are calculated at each sampling time. This optimal increment sequence minimizes the multistage cost function formulated in Eq. (21) within the area limited by hard constraints on input current, output SOC and terminal voltage simultaneously. Finally, the first value of the optimal control increment is extracted and the step-wise control input $i(k)$ at each sampling time can be calculated as

$$i(k) = i(k-1) + \Delta i(k) \tag{30}$$

where $\Delta i(k) = [1,0,\cdots,0] * [\,\Delta i_k \;\; \Delta i_{k+1} \;\cdots\; \Delta i_{k+N_c-1}]^T$.

The constrained GPC strategy for battery control is implemented through the following steps at each sampling time:

Step 1: Acquire the outputs of electric and thermal behaviours based on the thermoelectric model and estimate the parameters of the CARIMA model using the RLS with forgetting factor.

Step 2: Calculate the *j*-step predictions based on the online identified CARIMA model.

Step3: Employ a standard solver such as the interior point method to solve this quadratic programming problem and find the optimal incremental control current, considering the inequality constraints and extract the first value of the incremental current control sequence.

Step4: Feed the control signal to the actuators and the data vectors of outputs are shifted in preparation for the next sampling time.

## 5. Experiments

The accuracy of the improved thermal sub-model is first validated through a practical battery self-heating test. Then simulation tests are conducted to investigate the performance of the constrained predictive controller for battery charging proposed in section 4.3. In the simulation tests, the sampling time is $T_s = 1s$, and the CARIMA model is used as a predictor. The ambient temperature is chosen as 27 °C and the initial battery shell and interior temperatures are both chosen as 29 °C. Three simulation tests are conducted, including (i) tracking performance test with different GPC tuning parameters; (ii) test with different heat dissipation rates; (iii) test with different internal temperature set-points. The tests are further analysed to identify the most appropriate of the heat dissipation rates and proper internal temperature set-points for the designed charging control strategy.

When using CARIMA model as the predictive model in the GPC controller, a complex model with a large number of model terms will increase the model complexity and computation time. On the other hand, an oversimplified model suffers from low performance in terms of both generalization performance and accuracy thus it is vital to perform structural optimization for CARIMA model.

In this paper, we use the fast recursive algorithm (FRA) [33] to determine the order of $n_a$ and $n_b$. This can be one of the contributions in this paper to optimize the CARIMA model structure in the GPC controller. The FRA is a fast forward method to select the most significant terms and optimize the model structure [33]. The candidate terms in the CARIMA model are selected continuously according to the cost net contribution for which terms that make the maximum contributions. This selection procedure would stop based on the cost function criterion. And the Sum Squared Error (SSE) is used as the cost function criterion in this study.

The order of $n_a$ and $n_b$ are set to $n_a = n_b = 8$ initially. After the model structure optimization using the FRA method, the most significant terms in the CARIMA model can be selected. And the order are determined as $n_a = 4$ and $n_b = 5$ respectively. This brings some benefits such as the orders are declined so that the CARIMA model can be simplified with good performance and the computation time can be shorten in the design of GPC controller. The detailed description of the FRA algorithm could be referred to [33] and will be not presented in this paper due to page limit.

### 5.1 Practical validation of the thermal model

The same practical battery self-heating test run at 26.3°C as described in [26] is used to validate the improved battery thermal model. The load current and voltage are shown in Fig. 3(a) and the heat generation results using two different calculation approaches in Eq. (11) are compared in Fig. 3(b) respectively. The $dU_{OCV}/dT_{in}$ values given in [34] is applied here. It is clear that $Q_1$ which only considers Joule heat generated by the internal resistance, is smaller than $Q_2$ which considers the heat generation caused by the over-potentials and entropy change within the battery. To further explore the effects of these two different heat calculation approaches as well as the effect of the two forms of thermal dissipation rate $k_2$ on the battery thermal model accuracy, two case studies, including 1) $Q_1$ with constant $k_2$ and 2) $Q_2$ with time-varying $k_2$ are conducted to validate the battery thermal model. The model validation results are then compared.

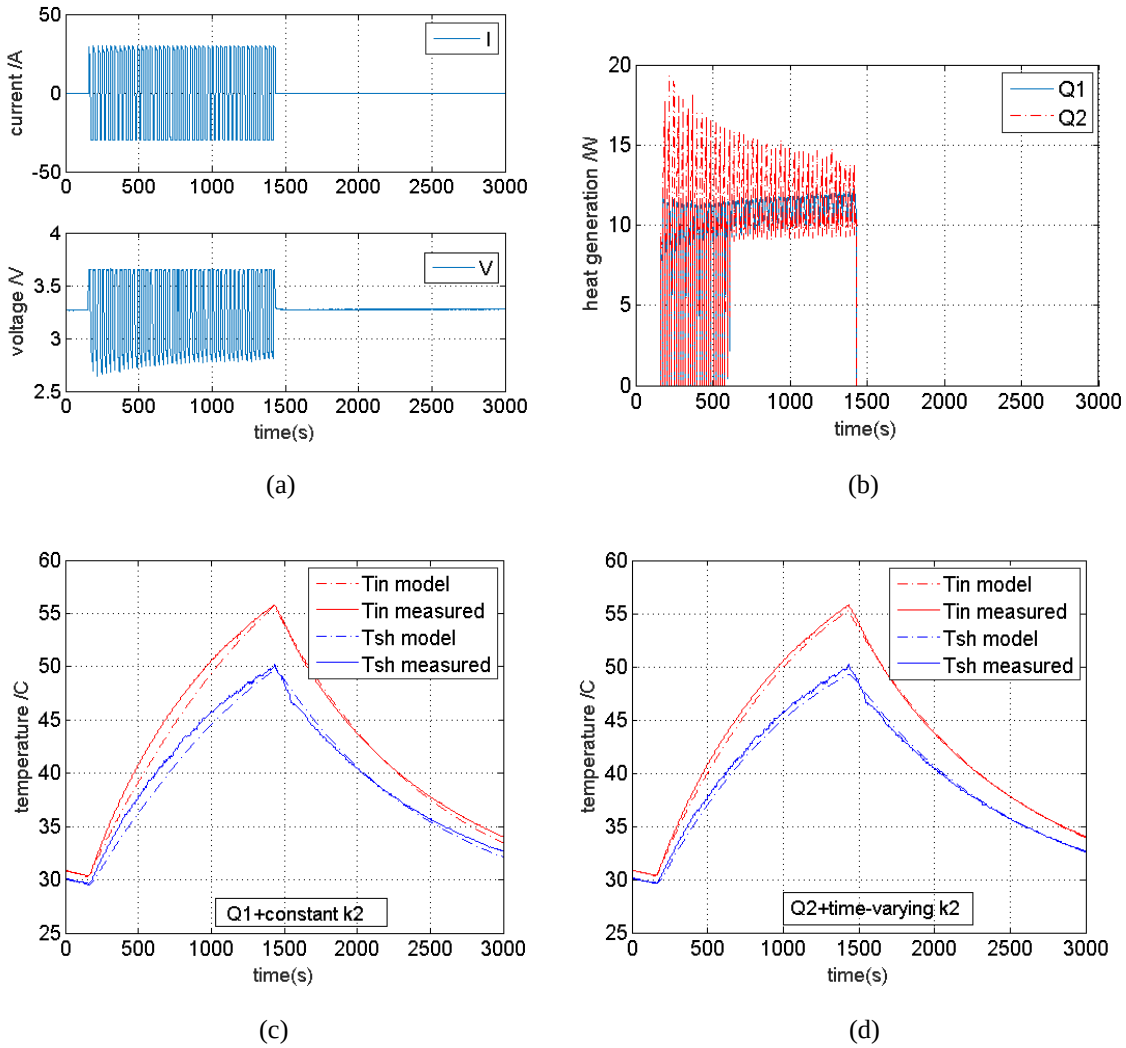


**Fig. 3.** Battery self-heating test and validation results for battery thermal model

The validation results for the thermal models are given in Fig. 3 (c) for $Q_1$ with constant $k_2$ and Fig. 3 (d) for $Q_2$ with a time-varying $k_2$, respectively. The validation results are summarized in Table 6. According to Table 6, it is clear that the thermal model accuracy is improved noticeably when $Q_2$ is used for the calculation of the heat generation while the thermal dissipation rate $k_2$ takes the time-varying form. Therefore, $Q_2$ and time-varying $k_2$ are adopted in the battery thermal model.

**Table 6.**
Validation test results for battery thermal model

| | $T_{in}$RMSE | $T_{in}$max error | $T_{sh}$RMSE | $T_{sh}$max error |
|---|---|---|---|---|
| $Q_1$+constant $k_2$ | 0.82℃ | 1.80℃ | 0.69℃ | 1.72℃ |
| $Q_2$+time-varying $k_2$ | 0.42℃ | 0.86℃ | 0.38℃ | 0.82℃ |

### 5.2 Tracking performance test with different control parameters

Parameters in the constrained GPC controller, including prediction horizon $N_P$ and penalty weight $R$ have huge impacts on the performance of the proposed battery charging control strategy. In order to test the effects of various parameters on control results and to achieve high efficiency control, $N_P$ and $R$ were varied while the control horizon and positive penalty weight for the output are fixed at $N_C$=2 and $Q = 1$ respectively in this test. The maximum charging current rate is chosen as 3C and the set-points of the battery internal temperature are fixed at 40°C.

The system responses with varying prediction horizon $N_P$ are shown in Fig. 4. These responses include the charge current as the control input and the corresponding controlled output variables (terminal voltage, internal temperature, shell temperature, SOC). It is shown that with the battery internal temperature control, the total battery charging time to bring SOC from 0.1 to the final targeted state 0.9 has increased to nearly 1500s compared with the CCCV profile in 1309 s due to the different charging current rate. The internal temperature is however maintained around 40°C. This allows the avoidance of the continuous rise of battery internal temperature. The surface temperature is also be maintained around 37.5°C. Since the battery surface temperature always reaches to a critical temperature more slowly than the internal temperature in the charging process, it is sufficient to control the internal temperature alone for battery charging thermal management.

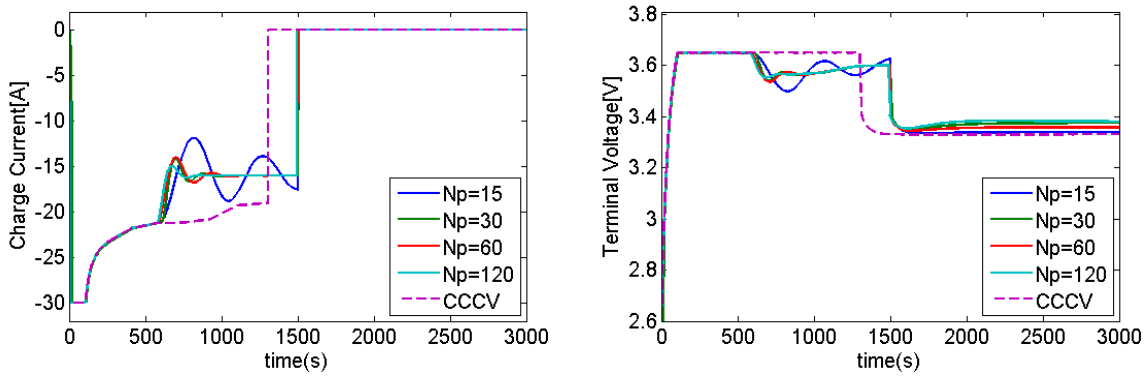


(a) (b)

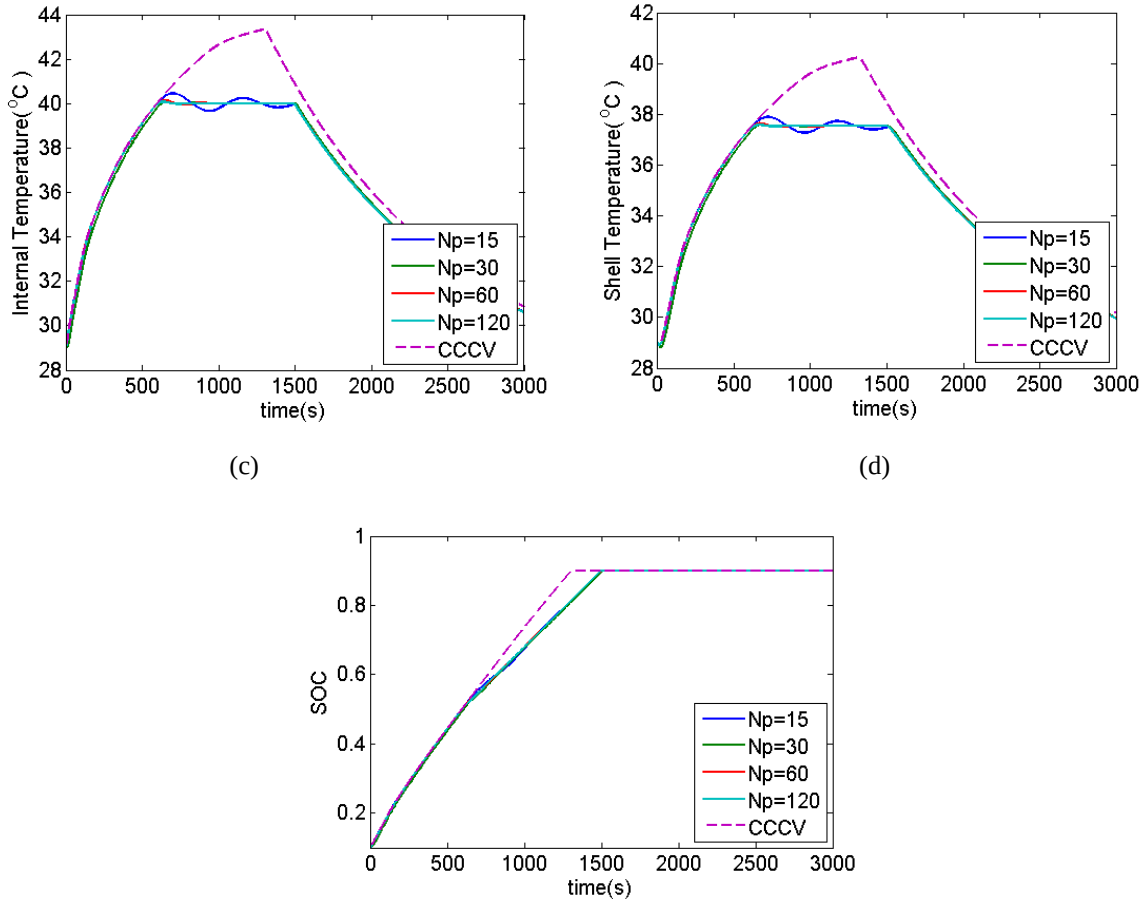


**Fig. 4.** Effect of the prediction horizon, $N_P$ ($N_c = 2, R = 1$)

The tests demonstrated that the control response speed is reduced for larger prediction horizon $N_P$. When $N_P$ is increased from 15 to 120, the charging profile become less steep and the charge current increment is smaller, and the output values are less fluctuated. But the larger $N_P$ will require more computing time for the GPC controller to calculate the corresponding incurrent increments. To balance the computing time and the fluctuations of the output values, we finally chose $N_P = 60$.

Fig. 5 illustrates the influence of the penalty weight $R$ choices on the control increment. Here the control horizon and the prediction horizon are fixed at $N_C$=2 and $N_P = 60$ respectively, only the penalty weight $R$ on the control increment for battery charging process is varied. The primary role for weight $R$ is to avoid control value change sharply. Reducing the value of $R$ can speed up the response for the battery internal temperature. When the control weight $R$ is increased from 0.05 to 1, the charging current changed slowly, leading to a slightly slow response for all output values, while the charging time with larger control weight $R$ is slightly longer, up to 1512s when control weight is chosen as $R = 1$. It should be noted that when the control weight $R$

is decreased below 0.05, the responses for battery charging process are almost the same, further decreasing it will not make any notable difference to the battery charging performance, therefore $R = 0.05$ is taken as the lower limit.

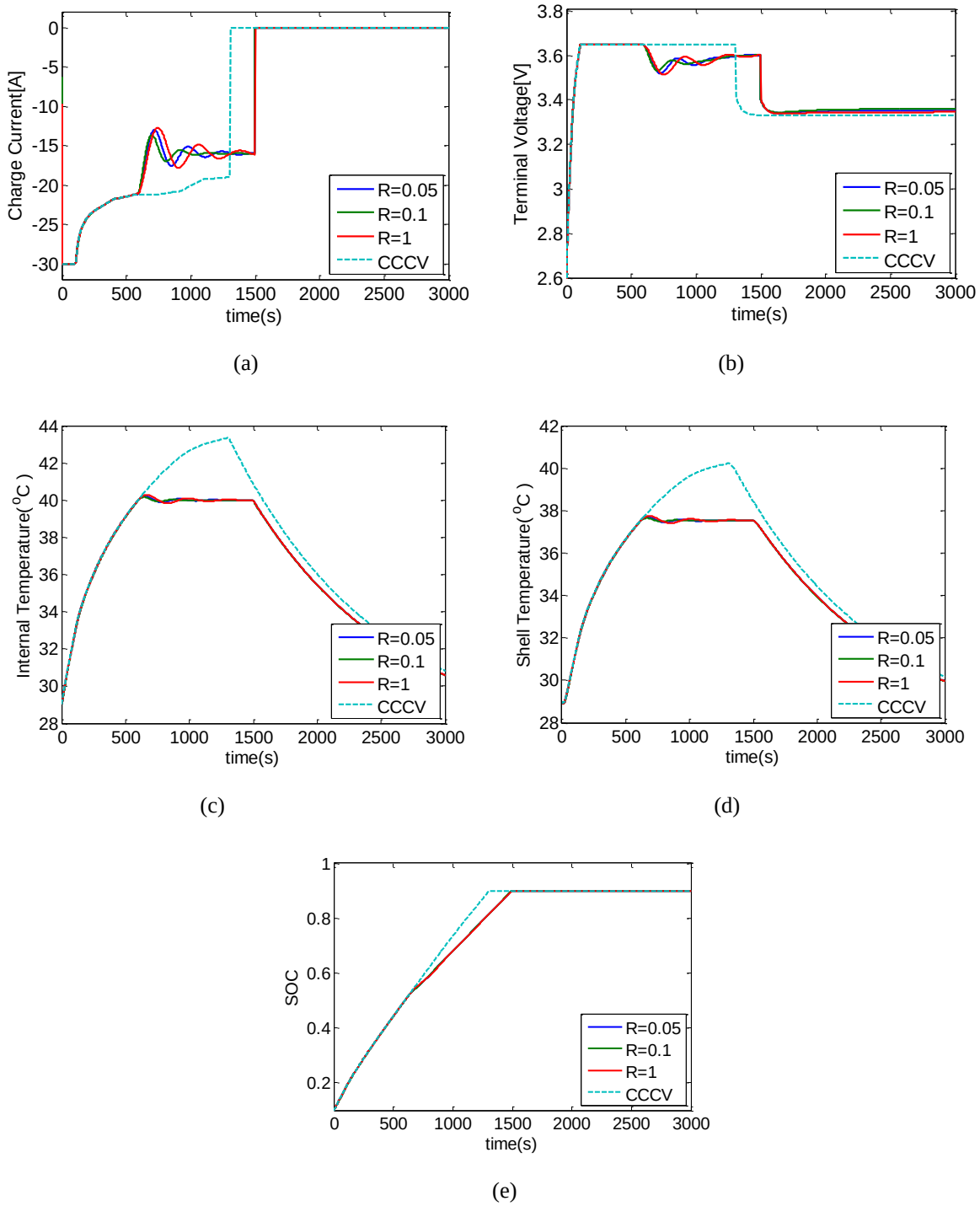


**Fig. 5.** Effect of control penalty weight, $R$ ($N_c = 2, N_P = 60$)

### 5.3 Heat dissipation rate test

The thermal dissipation rate $k_2$ in Eq. (12) stands for the heat conduction between the battery shell and the ambience which can be increased by active thermal management including air fan or liquid cooling system. $k_2$ is a compromise between the cooling cost and the dissipation efficiency (larger $k_2$ usually implies higher cost). In order to inspect the influence of different dissipation rates on the performance of the charging control strategy and further to find out the most appropriate region of $k_2$ for battery charging, the $k_2$ is varied while control parameters in GPC being fixed ($N_c = 2, N_P = 60, R = 0.05$) in this test. The internal temperature set-points are chosen as 40°C. The responses of output variables and the variation of charge current are shown in Fig. 6. It is evident that as $k_2$ decreases from 0.4 to 0.1, both the battery internal and surface temperatures increase more rapidly, and the charging time to bring SOC from 0.1 to the 0.9 become noticeably longer. This is mainly due to the reduced $k_2$ which implies less thermal convection occurring between the battery surface and the surrounding ambient circumstance. The charge current therefore had to be smaller in order to maintain internal temperature at a desirable level. It is clear that the thermal dissipation rate has a significant impact on the battery temperature, and a suitable thermal dissipation rate $k_2$ needs to be chosen which should balance the cost and charging time in battery charging process.

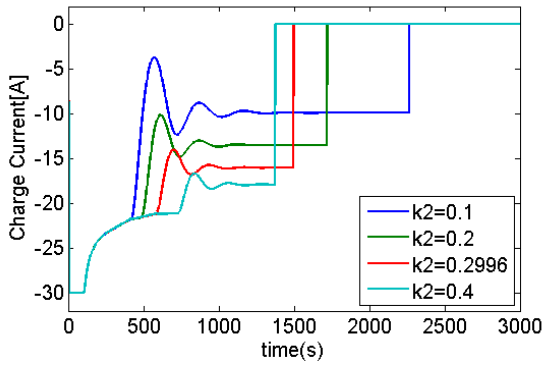


(a)

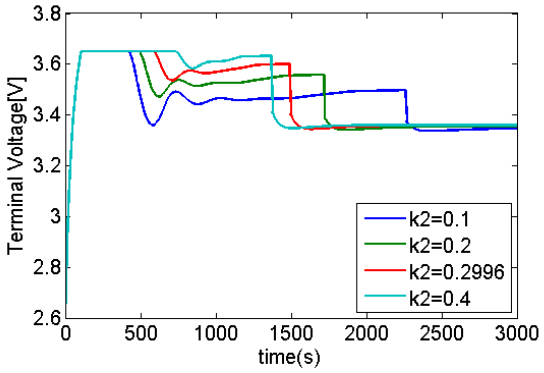


(b)

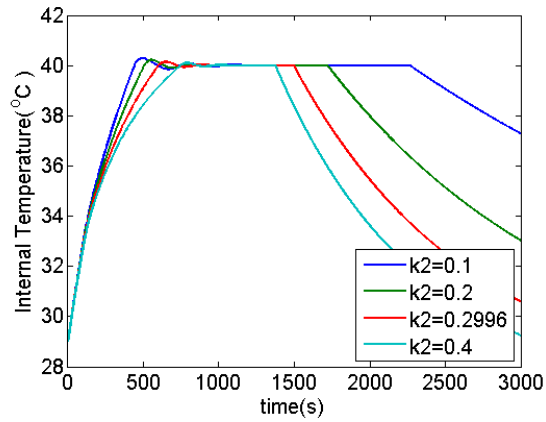


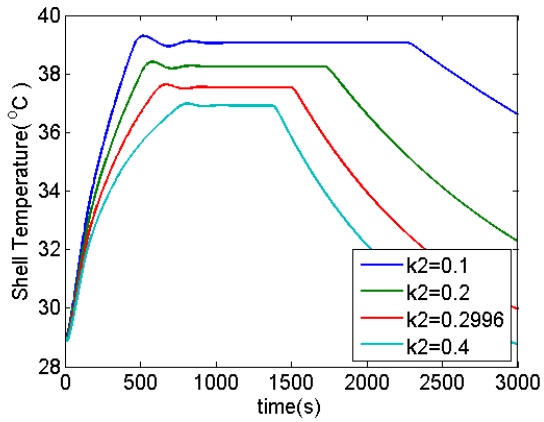

(c) (d)

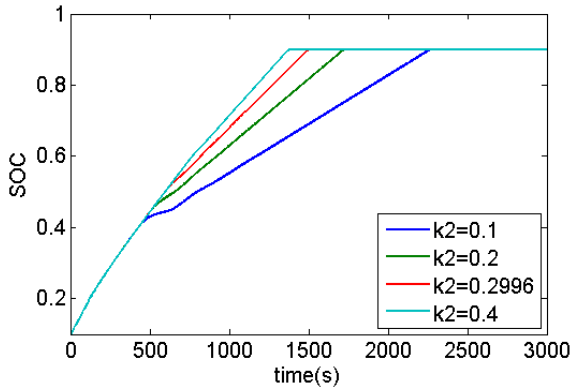


(e)

**Fig. 6.** Effect of different heat dissipation rates $k_2$ ($N_c = 2, N_P = 60, R = 0.05$)

Given this consideration and the above experimental results, we now suppose there is a linear relation between dissipation rate $k_2$ and cost, and a nonlinear relation between $k_2$ and the corresponding charging time in our battery control strategy. Then there must exist a region which further increase of $k_2$ does not significantly reduce the charging time. In order to find the most appropriate region for the dissipation rate $k_2$ in this case ($N_c = 2, N_P = 60, R = 0.05$), an experiment to find the effect of different dissipation rates on the charging time is conducted and the results are shown in Fig. 7. In the experiment, the parameter $k_2$ and the internal temperature set point $T_{in}$ are incrementally changed with a magnitude of 0.025 and 1°C respectively. We define the change of charging time $D_T$ as,

$$D_T(k_2^i) = T(k_2^i) - T(k_2^{i-1}) \tag{31}$$

where $T(.)$ stands for the response charging time with corresponding $k_2$. Then the change rate of charging time $R_T$ can be defined as,

$$R_T(k_2^i) = D_T(k_2^i) / T(k_2^{i-1}) \tag{32}$$

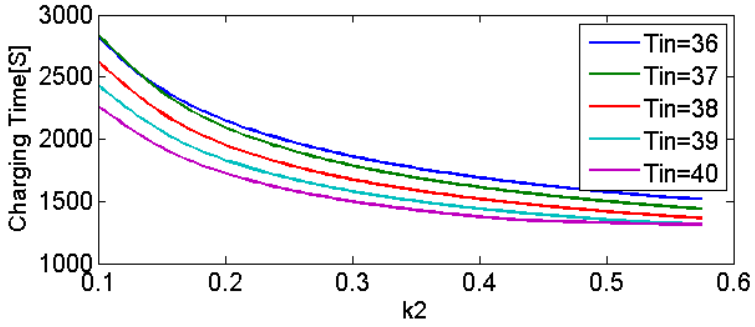

(a)

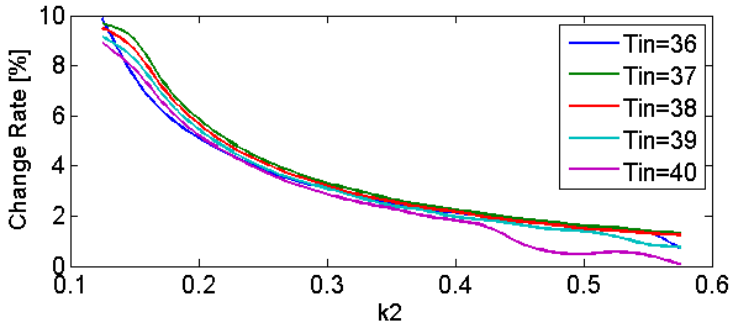


(b)

**Fig. 7.** Relations of charging time with dissipation rates.(a) Charging time (b) Change rate of charging time

From Fig. 7, the following observations can be reached.

**Observation 1:** According to Fig. 7(a), it can be observed that for a fixed set-point $T_{in}$, as the dissipation rate $k_2$ increases, the response charging time decreases. However, this correlation is nonlinear. At a certain point, further increase of the value of $k_2$ will have much less effect on reducing the charging time. This result reveals that there exists a best trade-off between the dissipation rate $k_2$ and the corresponding charging time.

**Observation 2:** In order to find out the most appropriate region for $k_2$, the correlation of the change rate of the charging time is further explored and shown in Fig. 7(b). It is found that the change rate is larger than 4% when $k_2$ is less than 0.3. After this value of 0.3, the change rate becomes smaller than 4% which means further increase $k_2$ has insignificant impact on further reducing the charging time. Suppose the relation between dissipation rate $k_2$ and the manufacturing cost is linear, the results from Fig. 7(b) can confirm that improper setting of the dissipation rate will only increase the manufacturing cost without any noticeable benefit on reducing the charging time. The dissipation rate $k_2$ between 0.1 and 0.3 would be the most appropriate region if we consider 4% as the acceptable change rate of the charging time.

### 5.4 Test of different internal temperature set-points

Another test is conducted to examine the influence of various internal temperature set-points on the battery charging process and the results are shown in Fig. 8. Then a cost function considering both the charging time and the energy loss is presented to find out the proper internal temperature target. In this test, five different battery internal temperature set-points (36ºC, 37ºC, 38ºC, 39ºC, 40ºC) are chosen. All of the five charging profiles show that the charging time are longer than the CCCV method as the charge currents have been

changed to keep battery internal temperature within the desirable level. At the beginning of the charging process, all charge currents are quite similar with the current profile using CCCV method as an effect to increase the SOC as quickly as possible. These same charge current profiles will last until the battery internal temperatures increase to the targeted temperature. There are then apparent differences in the charge current for different internal temperature targets. When the internal temperature target is reduced from 40 ºC to 36ºC, the charging time for different set-points is 1498s (40 ºC), 1579s (39 ºC), 1674s (38 ºC), 1786s (37 ºC) and 1918s (36 ºC) respectively. Low targeted internal temperature prolongs the battery charging time. Internal temperature target is a compromise between the battery charging time and energy loss (larger internal temperature target usually means less charging time but higher energy loss). It is therefore vital to select a proper internal temperature target in charging process to balance the battery charging time and energy loss especially in high power applications.

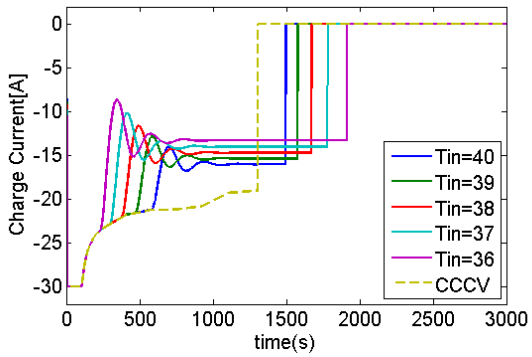


(a)

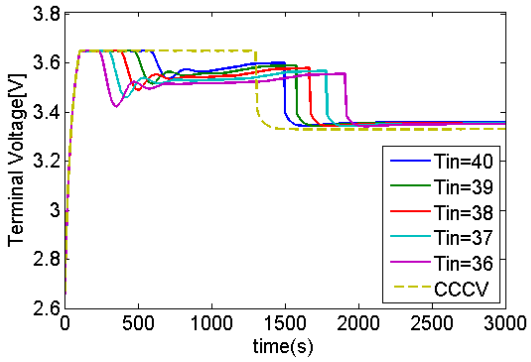


(b)

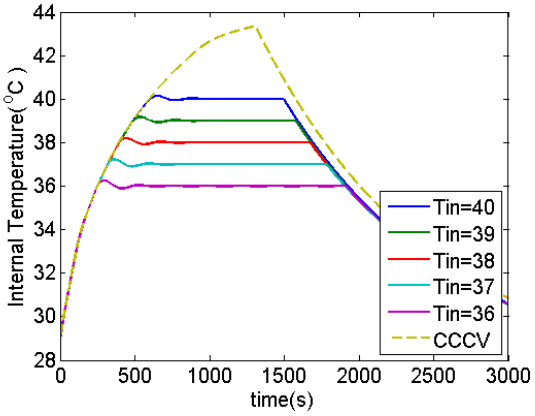


(c)

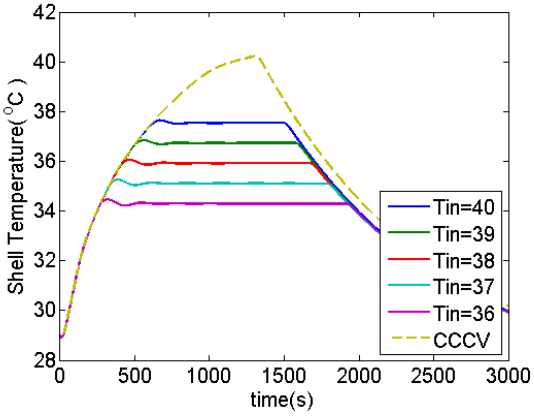


(d)

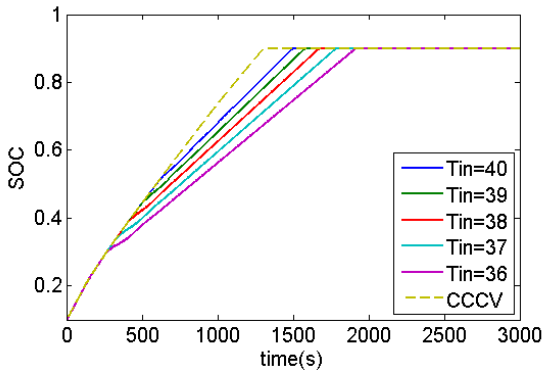


(e)

**Fig. 8.** Effect of different internal temperatures ($N_c = 2, N_P = 60, R = 0.05$)

Given this consideration, we can use a cost function to evaluate the performance during battery charging which combines both battery charging time and energy loss

$$J = (1 - a_1) * t_f + a_1 * \int_{t=0}^{t=t_f} i(t) * \left(V(t) - U_{OCV}(t)\right) + i(t) * T_{in}(t) * dU_{OCV}(t)/dT_{in}(t)\, dt \quad (33)$$

where $t_f$ stands for the time when battery reaches its final SOC level. $0 \leq a_1 \leq 1$ is the weighting factor to balance the two objective terms (charging time and energy loss).

In the experiment, we use a fixed value $a_1 = 0.25$ , and the cost functions for five charging profiles with different battery internal temperature targets (36ºC, 37ºC, 38ºC, 39ºC, 40ºC) are calculated and listed in Table 7. It is shown that if the internal temperature target is reduced, the battery charging time $t_f$ will increase but the energy loss will become less. The cost function $J$ decreases from 2952.46 (40ºC trajectory) to 2931.37 (37ºC trajectory) and then adversely increases to 2933.81 (36ºC trajectory). So the internal temperature target between 36ºC and 38ºC would give the best cost function value in this case. It is a trade-off between charging speed and energy loss for the selection of the internal temperature targets.

[Table 7 about here.]

## 6. Conclusion

Battery temperature especially the internal temperature is a key part of the battery thermal management in electric vehicles for battery operation safety and behaviour especially in high power applications. In this paper, a novel control strategy by applying the constrained GPC based on a new battery coupled thermoelectric model is proposed to maintain the $LiFePO_4$ battery internal temperature within a desirable level while achieving fast

charging. Hard constraints for terminal voltage, surface temperature, SOC and charging current are all integrated into the GPC controller design. To achieve this, an experimentally validated improved thermoelectric model is firstly used to capture both the battery electric and thermal behaviours simultaneously. Then based on the comprehensive formulation of the battery behaviours estimated by the thermoelectric model, a CARIMA model is proposed as the online self-tuning predictive model used in the GPC controller. The parameters of CARIMA model are identified by the RLS algorithm with forgetting factor to improve the robustness of GPC controller. Then the designed GPC controller is developed to control the charging current with different GPC tuning parameters, together with different heat dissipation rates and various internal temperature targets. The experiment results have confirmed the effectiveness of the proposed control strategy for battery thermal management. The most appropriate region for the heat dissipation rates and the proper internal temperature set-points are further investigated and analysed. This control strategy tackles simultaneous battery fast charging and internal temperature control, which are of significant importance in designing the battery thermal management system for EVs. The strategy can be easily implemented in other battery charging applications to manipulate the charge current for battery thermal management, guaranteeing charging efficiency and prolonging battery service lifetime.

## Acknowledgement

This work was financially supported by UK EPSRC under the 'Intelligent Grid Interfaced Vehicle Eco-charging (iGIVE) project EP/L001063/1 and NSFC under grants 51361130153, 61673256 and 61273040. Kailong Liu would like to thank the EPSRC for sponsoring his research.

## Reference

[1] Tie, S. F., C. W. Tan, A review of energy sources and energy management system in electric vehicles, Renewable and Sustainable Energy Reviews 20 (2013) 82-102.

[2] L. Lu, X. Han, J. Li, J. Hua, M, Ouyang, A review on the key issues for lithium-ion battery management in electric vehicles. Journal of power sources 226 (2013) 272-288.

[3] Z. Rao, S. Wang, A review of power battery thermal energy management, Renewable and Sustainable Energy Reviews, 15(9) (2011) 4554-4571.

[4] J. Jaguemont, L. Boulon, Y. Dubé, A comprehensive review of lithium-ion batteries used in hybrid and electric vehicles at cold temperatures. *Applied Energy* 164 (2016) 99-114.

[5] T. Bandhauer, S. Garimella, T. Fuller, A critical review of thermal issues in lithium-ion batteries, Journal of the Electrochemical Society, 158(3) (2011) R1-R25.

[6] Lee, Y. Shung, M. Cheng, Intelligent control battery equalization for series connected lithium-ion battery strings. Industrial Electronics, IEEE Transactions on, 52(5) (2005) 1297-1307.

[7] Maleki, Hossein, J. Selman, R. Dinwiddie, H. Wang, High thermal conductivity negative electrode material for lithium-ion batteries. Journal of power sources, 94(1) (2001) 26-35.

[8] M. Kise, S. Yoshioka, H. Kuriki, Relation between composition of the positive electrode and cell performance and safety of lithium-ion PTC batteries. Journal of Power Sources, 174(2) (2007) 861-866.

[9] Lee, Baek Haeng, and Sun Wook Kim, Development of battery management system for nickel–metal hydride batteries in electric vehicle applications. Journal of Power Sources 109(1) (2002) 1-10.

[10] J. Jang, S. Rhi, Battery thermal management system of future electric vehicles with loop thermosyphon, In Proceedings of the US–Korea conference on science, technology, and entrepreneurship (UKC), 2010.

[11] S. Khateeb, S. Amiruddin, M. Farid, J. Selman, S. Al-Hallaj, Thermal management of Li-ion battery with phase change material for electric scooters: experimental validation. Journal of Power Sources, 142(1) (2005) 345-353.

[12] M. Cosley, M. Garcia, Battery thermal management system, Telecommunications Energy Conference, INTELEC 2004. 26th Annual International. IEEE, 2004.

[13] C. Park, A. K. Jaura, Dynamic thermal model of li-ion battery for predictive behavior in hybrid and fuel cell vehicles. SAE Technical Paper, (2003) 2003-01-2286.

[14] X. Yi, Strategy and temperature affect of the charging of lithium-ion battery management system, International Conference on Applied Science and Engineering Innovation (ASEI 2015).

[15] E. Kim, K. G. Shin, J. Lee, Real-time battery thermal management for electric vehicles. In ICCPS'14: ACM/IEEE 5th International Conference on Cyber-Physical Systems (with CPS Week 2014), IEEE Computer Society, (2014) 72-83.

[16] J. Jiang, C. Zhang, C., J. Wen, W. Zhang, S. Sharkh, An optimal charging method for Li-ion batteries using a fuzzy-control approach based on polarization properties. Vehicular Technology, IEEE Transactions on, 62(7) (2013) 3000-3009.

[17] Y. Liu, C. Hsieh, Y. Luo, Search for an optimal five-step charging pattern for Li-ion batteries using consecutive orthogonal arrays, Energy Conversion, IEEE Transactions on, 26(2) (2011) 654-661.

[18] X. Hu, S. Li, H. Peng, F. Sun, Charging time and loss optimization for LiNMC and LiFePO4 batteries based on equivalent circuit models, Journal of Power Sources, 239 (2013) 449-457.

[19] R. Klein, N. Chaturvedi, J. Christensen, J. Ahmed, R. Findeisen, A. Kojic, Optimal charging strategies in lithium-ion battery, In American Control Conference (ACC), IEEE, (2011) 382-387.

[20] M. Xavier, M. Trimboli, Lithium-ion cell-level control using constrained model predictive control and equivalent circuit models. Journal of Power Sources, 285 (2015) 374-384.

[21] R. Richardson, P. Ireland, D. Howey, Battery internal temperature estimation by combined impedance and surface temperature measurement. Journal of Power Sources, 265 (2014) 254-261.

[22] M. Grimble, A. Ordys, Predictive control for industrial applications. Annual Reviews in Control, 25 (2001) 13-24.

[23] L. Liu, J. Park, X. Lin, A. Sastry, W. Lu, A thermal-electrochemical model that gives spatial-dependent growth of solid electrolyte interphase in a Li-ion battery. Journal of Power Sources, 268 (2014) 482-490.

[24] C. Zhang, S. Santhanagopalan, M. Sprague, A. Pesaran, Coupled mechanical-electrical-thermal modeling for short-circuit prediction in a lithium-ion cell under mechanical abuse. Journal of Power Sources, 290 (2015) 102-113.

[25] M. T. Srbik, M. Marinescu, R. F. Martinez-Botas, G. J. Offer, A physically meaningful equivalent circuit network model of a lithium-ion battery accounting for local electrochemical and thermal behaviour, variable double layer capacitance and degradation. Journal of Power Sources, 325 (2016) 171-184.

[26]C. Zhang, K. Li, J. Deng, Real-time estimation of battery internal temperature based on a simplified thermoelectric model. Journal of Power Sources, 302 (2016) 146-154.

[27] Battery Chargers and Charging Methods, 2016. URL, http://www.mpoweruk.com/chargers.htm

[28] W. Shen, T. Vo, A. Kapoor, Charging algorithms of lithium-ion batteries: An overview. In Industrial Electronics and Applications (ICIEA), 2012 7th IEEE Conference on (pp. 1567-1572). IEEE.

[29 ] A. Fotouhi, D. Auger, K. Propp, S. Longo, M. Wild, A review on electric vehicle battery modelling: From Lithium-ion toward Lithium–Sulphur. Renewable and Sustainable Energy Reviews, 56 (2016) 1008-1021.

[30] X. Hu, S. Li, H. Peng, A comparative study of equivalent circuit models for Li-ion batteries, Journal of Power Sources, 198 (2012) 359-367.

[31] X. Lin, H. E. Perez, J. B. Siegel, A. G. Stefanopoulou, Y. Li, R. D. Anderson, Y. Ding, M. P. Castanier, Online parameterization of lumped thermal dynamics in cylindrical lithium ion batteries for core temperature estimation and health monitoring. IEEE Transactions on Control Systems Technology 21(5) (2013) 1745-1755.

[32] H. Dai, L. Zhu, J. Zhu, X. Wei, Z. Sun, Adaptive Kalman filtering based internal temperature estimation with an equivalent electrical network thermal model for hard-cased batteries. Journal of Power Sources 293 (2015) 351-365.

[33] K. Li, J.-X. Peng, and G. W. Irwin, A fast nonlinear model identification method, Automatic Control, IEEE Transactions on, 50(8) (2005) 1211–1216.

[34] J. Sun, G. Wei, L. Pei, R. Lu, K. Song, C. Wu, C. Zhu, Online Internal Temperature Estimation for Lithium-Ion Batteries Based on Kalman Filter. Energies 8(5) (2015) 4400-4415.

## Tables

### List of Tables



**Table 1.**
Characteristics of $LiFePO_4$ battery [21]

| **LiFePo4 battery** | |
|---|---|
| **Voltage (nominal)** | 3.20V~3.30V |
| **Charge (C-rate)** | Charge to 3.65V (1C): typical 3 hours charge time |
| **Discharge (C-rate)** | 40A pulse ; 2.50V cut-off (lower than 2V may cause damage) |
| **Specific energy** | 90-120 Wh/kg |
| **Thermal runaway** | 270°C (518 °F) |
| **Cycle life** | 1000-2000 (related to depth of discharge, temperature) |
| **Applications** | Stationary and portable needing high endurance and load currents |
| **Comments** | Low capacity with very flat voltage discharge curve. One of the safest Li-ion batteries. |

**Table 2.**

Reasonable ambient temperature constraints for various batteries

| Battery Type | Charging Temperature | Discharge Temperature | Charge Advisory |
|---|---|---|---|
| **Li-ion** | 0°C to 45 °C (32 °F to 113 °F) | -20°C to 60 °C (-4 °F to 140 °F) | Good charge/discharge performance at higher temperature but may shorten battery life. Not permitted for charging below freezing. |
| **Lead acid** | -20°C to 50 °C (-4 °F to 122 °F) | -20°C to 50 °C (-4 °F to 122 °F) | Lower V-threshold by 3mV/ °C when hot. Charging at 0.3C or less below freezing. |
| **NiMH , NiCd** | 0°C to 45 °C (32 °F to 113 °F) | -20°C to 65 °C (-4 °F to 149 °F) | Charge acceptances at 45°C and 60°C are 70% and 45% respectively. Charging at 0.1C between –18°C and 0°C. Charging at 0.3C between 0°C and 5°C. |

**Table 3.**

Battery OCV and SOC relationship

| **SOC** | 0.900 | 0.798 | 0.695 | 0.593 | 0.491 | 0.389 | 0.287 | 0.186 | 0.085 |
|---|---|---|---|---|---|---|---|---|---|

| **OCV(V)** | 3.330 | 3.325 | 3.299 | 3.292 | 3.290 | 3.278 | 3.251 | 3.215 | 3.057 |
|---|---|---|---|---|---|---|---|---|---|

**Table 4.**

Battery $R_o$ and internal temperature $T_{in}$ relationship

| $T_{in}$ (°C) | -10 | 0 | 10 | 23 | 32 | 39 | 52 |
|---|---|---|---|---|---|---|---|
| $R_o$(ohm) | 0.0259 | 0.0180 | 0.0164 | 0.0152 | 0.0125 | 0.0124 | 0.0120 |

**Table 5.**

Parameter identification results for thermoelectric model

| Parameter | Value |
|---|---|
| $a_1$ | 0.981 |
| $b_1$ | $1.8e^{-4}$ |
| $C_1$ | 263.8 |
| $C_2$ | 31.2 |
| $k_1$ | 1.264 |
| $k_2$ | 0.33 |
| $k_{2,1}$ | 0.268 |
| $k_{2,2}$ | 0.0044 |

**Table 6.**

Validation results for battery thermal model part

| | $T_{in}$RMSE | $T_{in}$max error | $T_{sh}$RMSE | $T_{sh}$max error |
|---|---|---|---|---|
| $Q_1$+constant $k_2$ | 0.82℃ | 1.80℃ | 0.69℃ | 1.72℃ |
| $Q_2$+time-varying $k_2$ | 0.42℃ | 0.86℃ | 0.38℃ | 0.82℃ |

**Table 7.**

Battery cost function $J$ and its terms under different trajectories $T_{in}$

| $T_{in}$ (°C) | 40 | 39 | 38 | 37 | 36 |
|---|---|---|---|---|---|
| $J$ | 2952.46 | 2939.03 | 2933.73 | 2931.37 | 2933.81 |
| $t_f$[s] | 1498.21 | 1579.73 | 1674.48 | 1786.28 | 1906.36 |
| Heat[w] | 7315.21 | 7016.75 | 6711.48 | 6366.64 | 6016.16 |

## Figures

### Figures captions



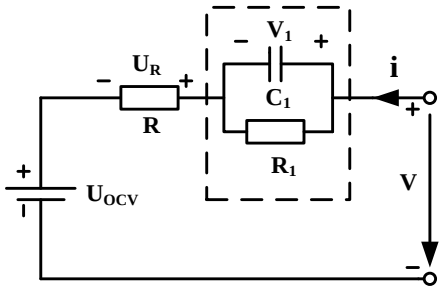


**Fig. 1.** Battery Thevenin model.

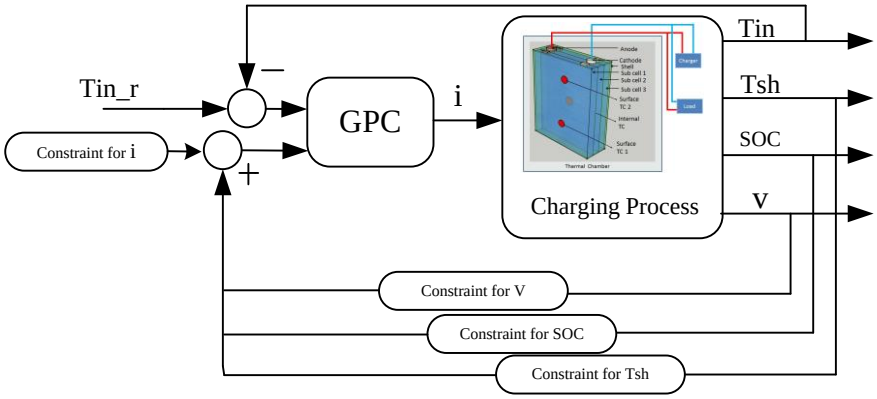


**Fig. 2.** Constrained GPC for battery charging

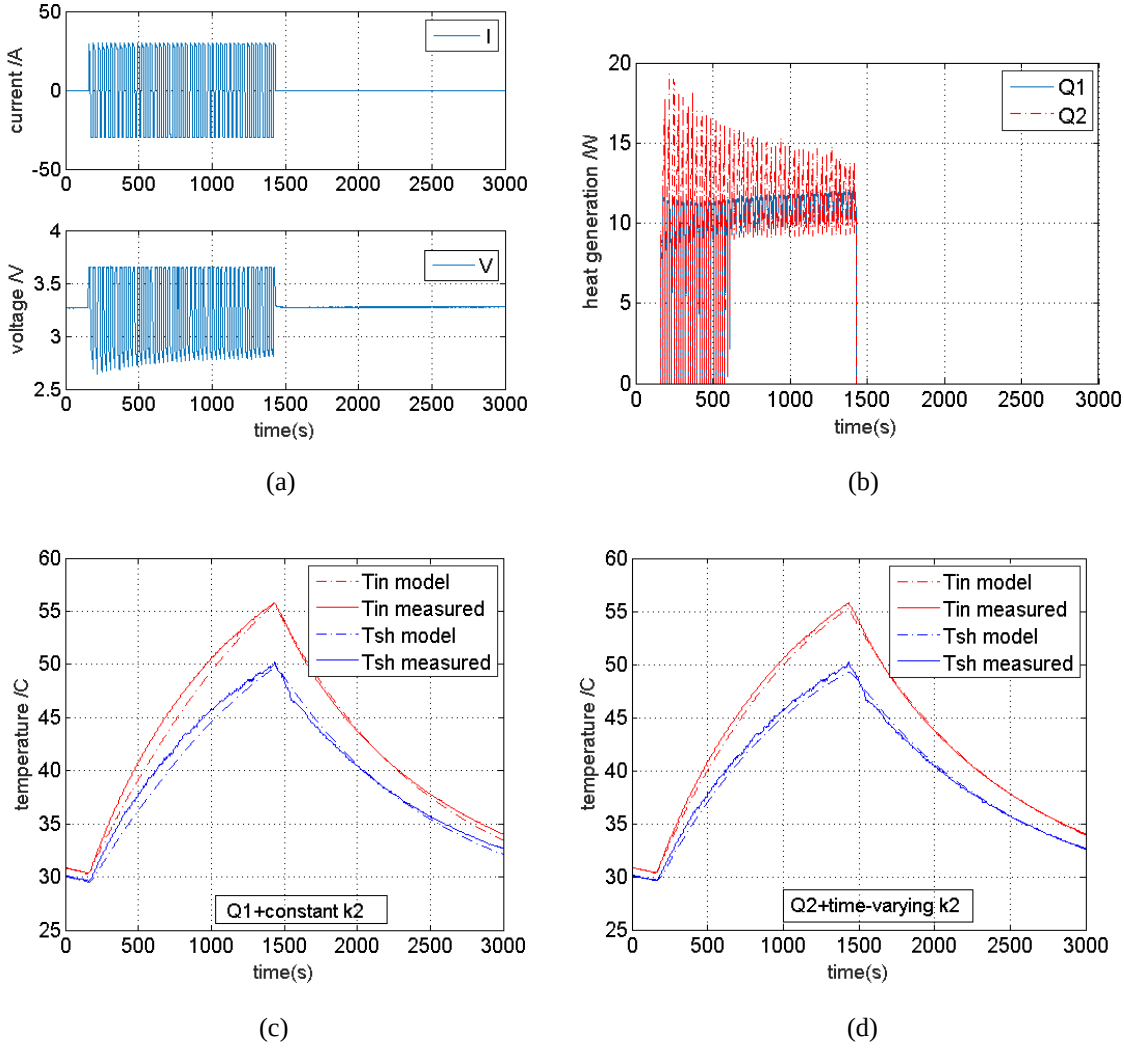


**Fig. 3.** Battery self-heating test and validation results for battery thermal model

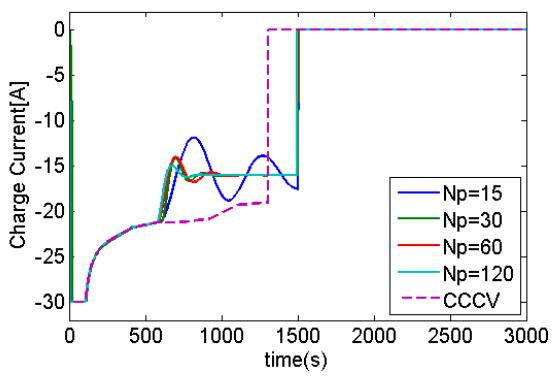


(a)

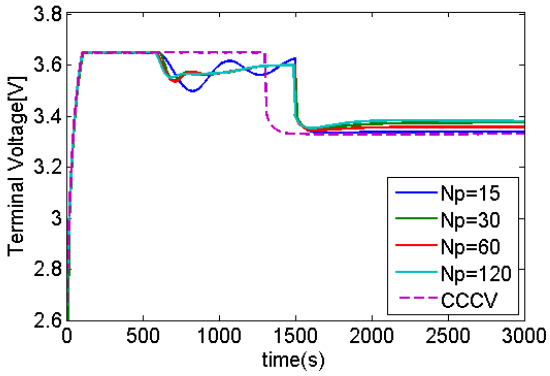


(b)

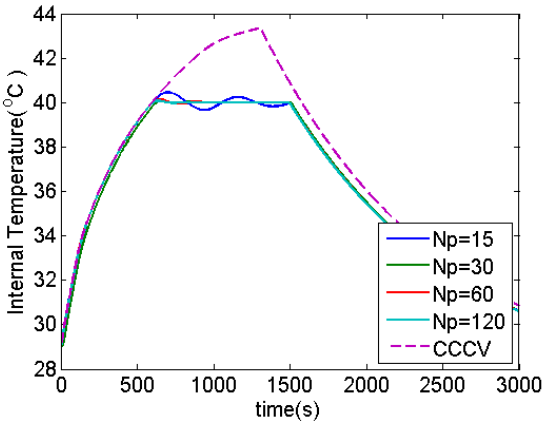


(c)

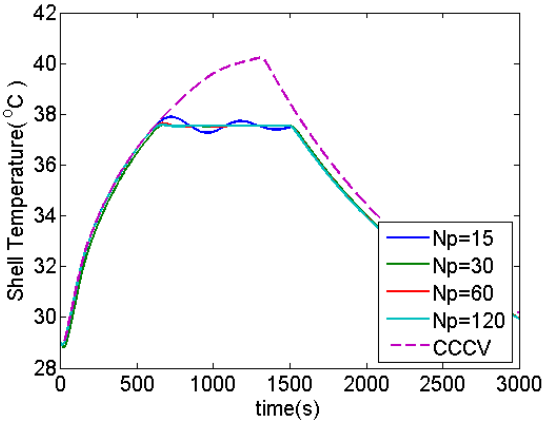


(d)

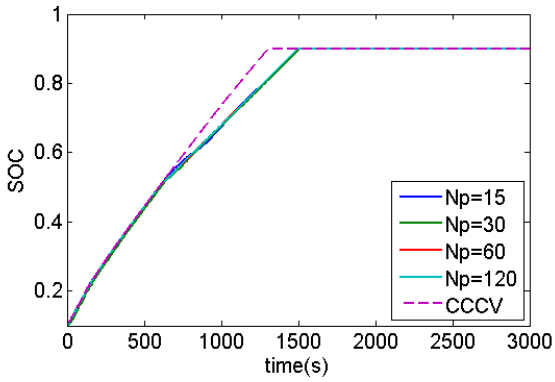


(e)

**Fig. 4.** Effect of the prediction horizon, $N_P$ ($N_c = 2, R = 1$)

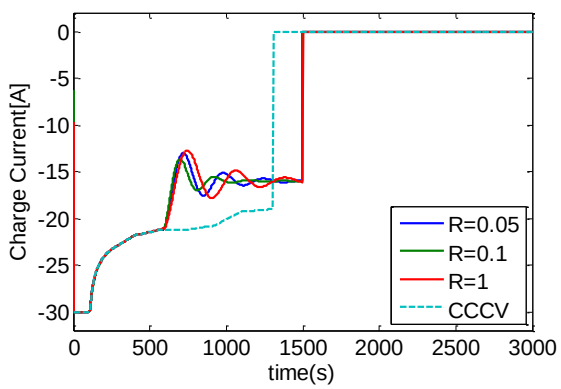


(a)

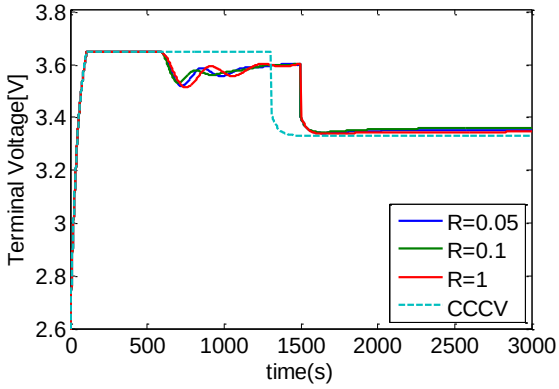


(b)

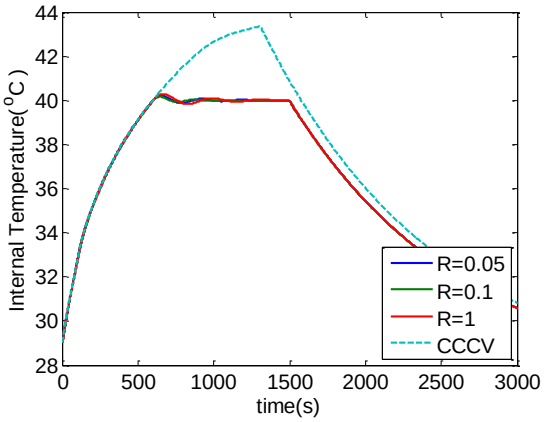


(c)

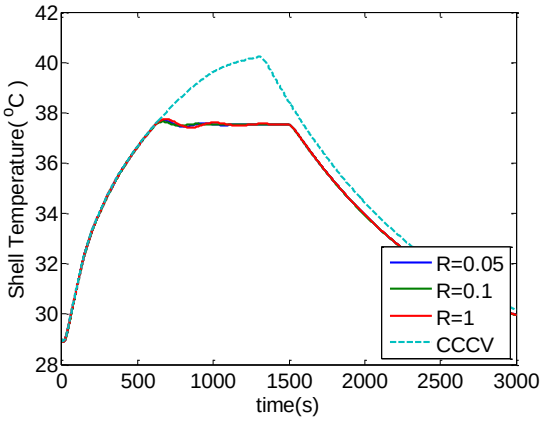


(d)

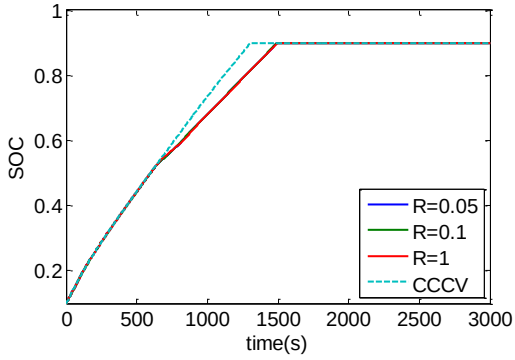


(e)

**Fig. 5.** Effect of control penalty weight, $R$ ($\mathrm{N_c} = 2, \mathrm{N_P} = 60$)

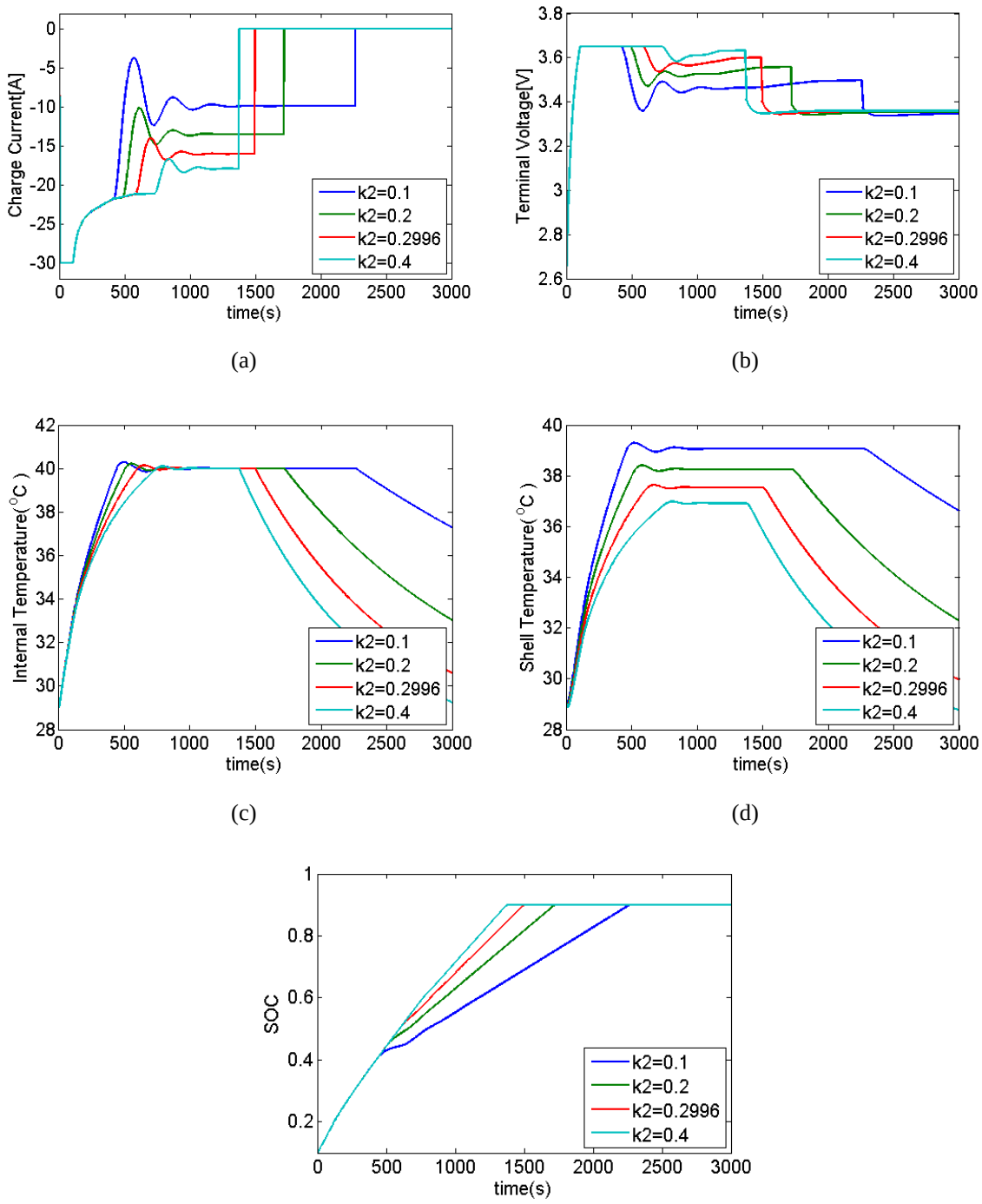


**Fig. 6.** Effect of different heat dissipation rates $k_2$ ($\mathrm{N_c} = 2, \mathrm{N_P} = 60, \mathrm{R} = 0.05$)

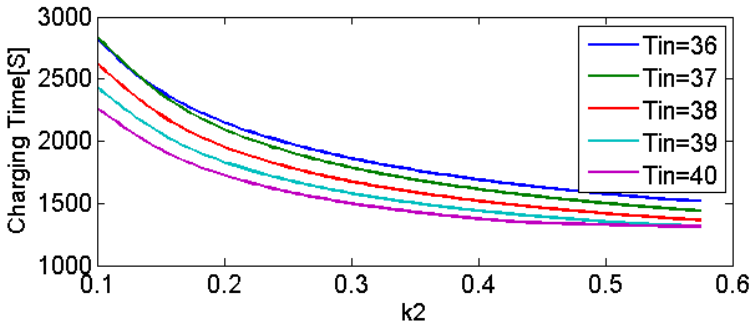


(a)

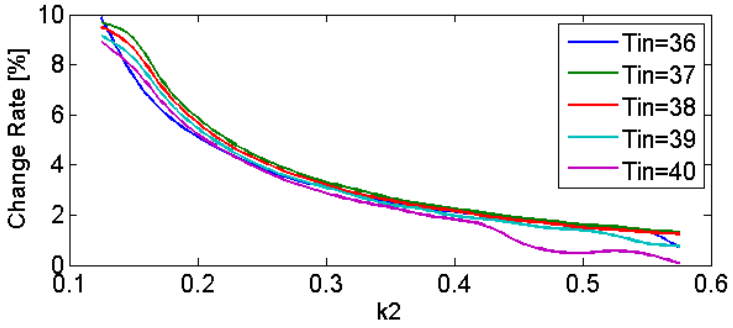


(b)

**Fig. 7.** Relations of charging time with dissipation rates.(a) Charging time (b) Change rate of charging time

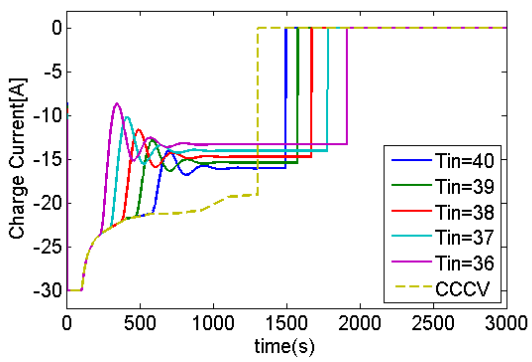


(a)

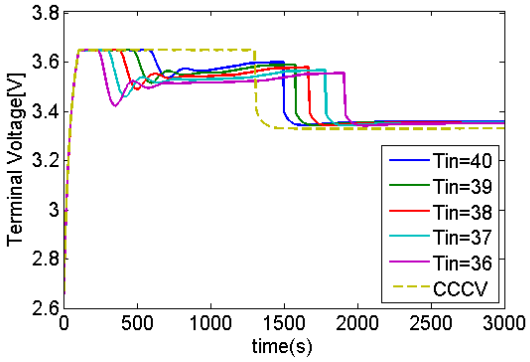


(b)

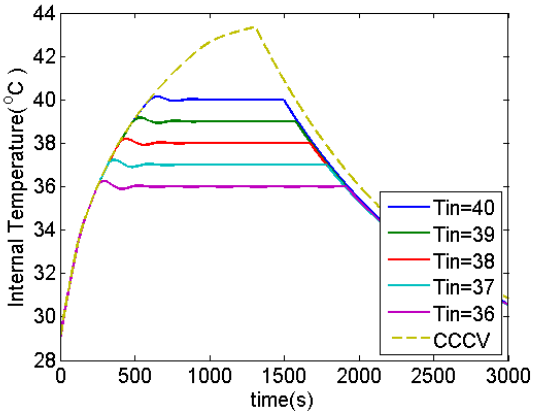


(c)

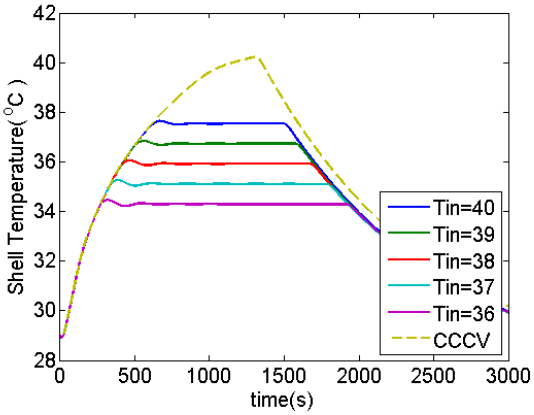


(d)

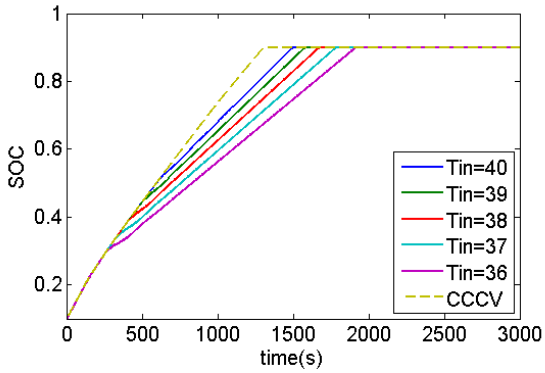


(e)

**Fig. 8.** Effect of different internal temperatures ($N_c = 2, N_P = 60, R = 0.05$)